processes

MDPI

Review

Recent Advances in Biochar-Based Hydrogel Composites: Preparation, Aquatic Environmental Applications, and Adsorption Mechanisms

Yuxin Zhao [1], Chaojie Wang [2], Qing Han [2], Zheng Fang [2,*], Yurong Gao [3], Hanbo Chen [4], Jianhong Li [5], Xing Yang [6], Junfeng Chen [7] and Hailong Wang [2,*]

1 School of Materials and Energy, Foshan University, Foshan 528000, China; 2112206012@stu.fosu.edu.cn
2 School of Environmental and Chemical Engineering, Foshan University, Foshan 528000, China; 2112360035@stu.fosu.edu.cn (C.W.); 2112460057@stu.fosu.edu.cn (Q.H.)
3 School of Environmental Science and Engineering, Guangzhou University, Guangzhou 510006, China; yurong.gao@foxmail.com
4 Key Laboratory of Recycling and Eco-Treatment of Waste Biomass of Zhejiang Province, School of Environment and Natural Resources, Zhejiang University of Science & Technology, Hangzhou 310023, China; chenhanbo1225@zust.edu.cn
5 Rubber Research Institute, Chinese Academy of Tropical Agricultural Sciences, Haikou 571101, China; ljh0302@163.com
6 Key Laboratory of Agro-Forestry Environmental Processes and Ecological Regulation of Hainan Province, School of Environmental Science and Engineering, Hainan University, Haikou 570228, China; xing.yang@hainanu.edu.cn
7 School of Life Science, Qufu Normal University, Qufu 273165, China; chenjunfeng@qfnu.edu.cn
* Correspondence: fangzheng-environ@foxmail.com (Z.F.); hailong.wang@fosu.edu.cn (H.W.)

Abstract: In the face of the escalating crisis of water pollution, biochar-based hydrogel composites (BCGs) have emerged as a promising material for water treatment, owing to their distinctive performance and environmental friendliness. These composites combine the high specific surface area and porous structure of biochar with the three-dimensional network of hydrogel, demonstrating superior adsorption capacities and ease of recyclability within aquatic systems. This paper provides the first overview of BCGs synthesis methods, with a particular emphasis on encapsulation and co-pyrolysis techniques. Furthermore, the environmental applications of BCGs are summarized, focusing on their efficacy and mechanisms in the removal of organic contaminants, heavy metals, and nutrients from water bodies. Our analysis underscores the pivotal role of BCGs in environmental preservation and pollution mitigation efforts, suggesting that its implementation could lead to a significant advancement in water pollution abatement strategies.

Keywords: aquatic contaminants; encapsulation; co-pyrolysis; adsorption; mechanism

Received: 10 January 2025
Revised: 12 February 2025
Accepted: 21 February 2025
Published: 26 February 2025

Citation: Zhao, Y.; Wang, C.; Han, Q.; Fang, Z.; Gao, Y.; Chen, H.; Li, J.; Yang, X.; Chen, J.; Wang, H. Recent Advances in Biochar-Based Hydrogel Composites: Preparation, Aquatic Environmental Applications, and Adsorption Mechanisms. *Processes* **2025**, *13*, 664. https://doi.org/10.3390/pr13030664

1. Introduction

Nowadays, the demand for CO_2 emission reduction, resource regeneration, and environmental protection is urgently increasing, which draws huge attention from researchers and ordinary people. The primary strategies for environmental remediation include photocatalysts, sensing, adsorption, fertilizer, and pesticides [1–3]. Among them, adsorption stands out for its economic viability, efficiency, and operational simplicity [4]. Bearing the advantages of negative CO_2 emission, reuse of biomass wastes, low cost, high specific surface area [5–10], porous structure [5–8,10–16], and ample surface functional groups [5,7,10,17,18], biochar has triggered explosive research interests in recent years [19–21]. Generally, the feedstock of biochar, possessing the advantages of extensive sources, low cost, and environment friendliness, stems

from carbon-enriched biomass such as forestry and agricultural waste [6,15,22], industrial rubbish [15], and animal manure [10,22]. Resulting from its intriguing physicochemical properties and significant meaning in environment protection, waste management, and ecological preservation, biochar has played an essential role in addressing environmental pollution in recent years, such as aquatic and soil remediation [19,23]. Biochar and its modifications have shown promising removal capability toward various environmental contaminants [16–18], such as anionic and cationic dyes [24], organic pesticides [25], oils [26], micropollutants [2], and heavy metals [27].

However, the large-scale application of biochar in water treatment may be limited by the particulate form of biochar [7]. Usually, biochar is prepared in powder form [13], which is prone to agglomeration, leading to a much-lowered adsorption capacity. The problem of ease of migration and loss, the difficulty of recovering and collecting, unsuitability for long-term effective disposal, and need for additional separation cost could all exist in the application of wastewater treatment [8,11,16,28,29]. Furthermore, when biochar-based adsorbents are used in continuous industrial applications, their powder nature may lead to column clogging [8].

The probable leaching and run-off of water-soluble active elements such as metal oxide/sulfide and P from modified biochar-based adsorbents is also a potential problem, which could result in secondary contamination issues [7,30]. Therefore, methods that can screen the leaching of metal ions are vital to the practical applications of biochar-based adsorbents. In the past few years, the adsorption, modification, and multifunctional application of biochar has been well reviewed [5,19,20,31]. The exploration of novel modification methods has attracted enormous research interest and endeavors in recent years. Hydrogel embedding may be a useful approach to solving the aforementioned problem.

Hydrogel is a type of hydrophilic material possessing unique three-dimensional networks [32] and high pore volume [10] and is widely applied in industrial, medical, and environmental applications [15]. It is reported that many precursors, such as cellulose [33], alginate [34], chitosan [4], lignin [35], and graphene oxide [27], could be used to prepare hydrogel [15]. Possessing so many advantages, hydrogels are emerging as a significant class of excellent adsorbents for treating water and soil pollution and have shown high adsorption ability toward various pollutants, such as dyes, oils, and heavy-metal ions [36]. Biochar can be homogeneously distributed in a porous bulk hydrogel [37]. More importantly, the hydrogel can act as an external protector in biochar-based hydrogel composites (BCGs), which could efficiently reduce the adverse effects of the aforementioned biochar [30].

Note that immobilization of the powdered biochar-based materials into suitable gel medium to prepare BCGs could endow some unique performances and increase its prospect of practical application. For example, physicochemical properties such as maximum Young's modulus and plastic deformation resistance could be enhanced by the incorporation of biochar into hydrogel networks [37]. Furthermore, the reaction rate can be improved after the encapsulation of biochar into hydrogel due to the resulting enhanced conductivity after modification [32]. A larger specific surface area and more oxygen-containing functional groups and amino groups improved selective adsorption capacity toward pollutants, and convenient reusability could also be achieved by BCGs [13,17,18]. Therefore, compared to biochar, BCGs are generally characterized by higher adsorption capacity, faster adsorption kinetics, and enhanced selective adsorption capabilities. Furthermore, the leaching of metal ions from BCGs is effectively mitigated by the hydrogel matrix through physical encapsulation and chemical bonding. The three-dimensional network structure of the hydrogel restricts the diffusion of metal ions, while its surface functional groups (e.g., carboxyl and hydroxyl groups) enhance metal ion chelation via chelation mechanisms [38,39]. Furthermore, the feasibility of surface functionalization and other modification techniques

is improved by the hydrogel matrix, thereby enhancing the adsorption capacity and stability of BCGs. For instance, defects on graphene monolayers can be utilized to strengthen the anchoring of FeOx on the biochar surface, increasing the number of surface active sites and subsequently improving the pollutant immobilization capability of BCGs [27]. Although BCGs demonstrate promising potential for aquatic environmental remediation, their preparation process remains complex, involving biochar production, hydrogel synthesis, and their subsequent integration, often requiring additional processing and modification steps, which results in high production costs. Furthermore, precursors such as cellulose, alginate, chitosan, and lignin, which are used for BCG preparation, may gradually degrade during repeated use due to their biodegradability, leading to diminished adsorption performance in aquatic environments [39–41]. As a result, the quantitative and accurate assessment of the long-term efficacy and stability of BCGs continues to pose significant challenges. Additionally, current research on BCGs is largely confined to laboratory-scale studies, necessitating further expansion of its application scope in practical water treatment scenarios. Future research should focus on developing efficient and cost-effective production processes for BCGs to reduce their application costs in pollutant adsorption. Simultaneously, the adsorption performance and stability of materials both need to be further optimized to enhance their adaptability and reusability under diverse aquatic conditions.

Up to now, there have been a series of reviews about powder biochar concentrating on environmental applications such as water treatment and soil remediation. Regarding biochar with a three-dimensional network structure, to the best of our knowledge a comprehensive overview is still absent, especially for its application regarding environmental issues. Thus, an overview of the recent advances in BCGs for water treatment is provided in the present review. The link between the preparation, structure, environmental applications, and mechanisms of BCGs is highlighted. Furthermore, the synthetic methodologies of BCGs are first summarized. The interplay between material properties and the environmental performance of BCGs is comprehensively discussed, mainly to provide a theoretical basis and technical guidance for BCG design and their applications in environmental protection.

2. Preparation of BCGs

The preparation of BCGs can be achieved through two primary methods: encapsulation and co-pyrolysis (Figure 1). The encapsulation method involves dispersing biochar within a hydrogel precursor, followed by crosslinking and subsequent drying to form stable BCGs. This technique is straightforward and effective for maintaining the biochar's structure within the hydrogel matrix. In contrast, the co-pyrolysis approach integrates biochar and hydrogel components during the pyrolysis process under controlled conditions. This method allows for the development of a homogeneous carbonaceous matrix, enhancing the interaction between biochar and hydrogel. The main preparation parameters and material properties of BCGs are detailed in Tables 1 and 2, respectively. The primary gel matrixes for BCGs include cellulose, alginate, chitosan, lignin, and graphene, which will be introduced separately below (Figure 2).

Table 1. The preparation parameters and physicochemical properties of BCGs prepared by the encapsulation.

Materials	Gelation Process	SSA (m^2 g^{-1})	Mineral Facies	Morphology Features	Functional Group	Thermostability (TMLR)	pH_{PZC}	Ref.
CMC/guar gum/$KMnO_4$-modified biochar	Mixed KOH solution, AA, CMC, guar gum, and $KMnO_4$-modified biochar, added KPS and MBA, ultimately heated in a water bath, and then dried.	-	-	Honeycomb porous structure.	O-H, N-H, C=O, and -COOH.	45.50%	-	[42]
Alginate/biochar	Biochar was dispersed into the alginate solution, then dripped into the $CaCl_2$ solution, and finally dried.	242.34	-	Rough and irregular structure.	The surface is endowed with -OH, C=C, C-O, and C=O.	-	8.42	[29]
Fe-modified alginate/biochar	Biochar was mixed into a sodium alginate solution, then dropped into Fe^{3+} solution, concluding with freeze-drying.	2.32	The C peak of BC was retained, and the majority of Fe^{3+} within the hydrogel served to cross-link alginate molecules.	Visible protrusions and folds; BC can infiltrate the hydrogel matrix.	A substantial rise in oxygen-bearing functional groups is observed relative to BC.	-	3.8	[32]
Alginate/$KMnO_4$-modified biochar	Alginate and $KMnO_4$-modified biochar were mixed, then dropped into a $CaCl_2$ solution, and ultimately freeze-dried.	27.34	The resulting peaks corresponded to $CaCl_2$, H_2O, $Ca_{10}(PO_4)_6(OH)_2$, $KCaPO_4$, and MnO_2.	3D pore structure; biochar particles dispersed across the pore framework and the external surface.	Loading with alginate introduced a novel phenolic hydroxyl functional group.	-	1.5	[43]
Alginate/magnetic biochar	Alginate and magnetic biochar were combined, then immersed in $CaCl_2$ solution, and ultimately dried.	262.40	Amorphous structure and Fe_3O_4 particle diffraction peak.	Rough surfaces.	C=O, C-O-C, and Fe-O were observed.	-	6.5	[34]
Alginate/hydroxyapatite-modified biochar	Combined alginate and hydroxyapatite-modified biochar, then dripped into the $CaCl_2$ solution, and finally freeze-dried.	-	The resulting peaks corresponded to crystal plane diffraction peaks of hydroxyapatite.	The surface is smooth	The surface is rich in C-C, C-O, C=O, and P-O.	-	7.79	[44]
Chitosan/nZVI-modified biochar	Chitosan in 2% acetic acid, added /nZVI-modified biochar, and GA, finally, freeze-dried.	0.86	$2\theta = 21.3°$ represents the structure of crystalline chitin.	nZVI and BC pores were enveloped with chitosan in a sugar-coated layer.	The surface is enriched with hydroxyl and amino groups.	83.9%	6.5	[45]
N-doped graphene oxide/Fe-modified biochar	Mixed Fe-modified biochar and GO, added ethylenediamine, heated at 80 °C, and dried.	398.05	-	3D porous network structure.	Encapsulation of GO enhances functional group vibrational peak intensities.	86.00%	3.0	[15]
Reduced graphene oxide/KOH-modified biochar	Mixed KOH-modified biochar suspension with GO. solution, added ethylenediamine, reacted at 120 °C, and freeze-dried.	-	Hydrogen bonding exists between rGO and BC.	3D porous interconnected network structure.	C=O,C=C,C-H,C-O-C,C-OH and C-N-H were observed.	-	-	[10]

Table 1. *Cont.*

Materials	Gelation Process	SSA (m^2 g^{-1})	Mineral Facies	Morphology Features	Functional Group	Thermostability (TMLR)	pH_{PZC}	Ref.
Gellan gum/biochar	Gellan gum and polyvinyl alcohol were dissolved separately and then mixed; pre-treated biochar and glycerol were added and the mixture was poured into petri dishes and dried in a vacuum oven.	134.00	-	The surface of the material is irregular, exhibiting aggregates and sheet-like structures.	The surface is abundant in oxygen-containing functional groups.	72.05%	6.43	[46]
Starch/biochar	Biochar was dispersed in ethanol, while starch was dissolved in acetic acid; the mixture was combined with glycerol, then heated at 80 °C and dried.	226.94	-	3D network structure.	The surface exhibits -OH, nitro, C-O, and C=O.	98%	4.0	[17]
Polyacrylamide/MnO_2 modified biochar	AM, MBA, and MnO_2 modified biochar were combined, ball-milled, and mixed with sodium dodecyl sulfate to create foam, then TMEDA and $Na_2S_2O_8$ were added in sequence, followed by freeze-drying.	31.17	-	Dense and homogeneous microstructure.	Hydrogen bonds mediate the interaction between hydrogel (N-H) and BC (-OH).	38.00%	-	[37]
Polyacrylamide/ZnO-modified biochar	Under N_2, AM was combined with ZBC, followed by the addition of MBA, APS, and TEMED; then freeze-drying occurred after heating in a water bath.	-	-	Interconnected porous network, distribution of folds and nanoparticles on the surface.	Hydrogen bonding interactions between the N-H of hydrogel and the O-H of biochar.	63.83%	-	[47]
$CoFe_2O_4$/ starch-gelatin/MoO_3 modified biochar	Esterified corn starch was mixed with gelatin and microwaved, then $CoFe_2O_4$ and GA were added; after drying, it was mixed with MoO_3 modified biochar, ground, and microwaved.	-	2θ = 26.57, 42.74, 48.62° peaks indicated that $CoFe_2O_4$/starch-gelatin hydrogel was grafted with MoO_3 modified biochar.	3D porous network structure.	Nucleophilic substitution reaction between esterified corn starch and gelatin assisted by GA.	-	-	[48]

pH_{pzc} = pH value at the point of zero charge; SSA = specific surface area; TMLR = total mass loss rates; GA = glutaraldehyde; MBA = N, N'-methylene bis-acrylamide; APS = ammonium persulfate; TEMED = N, N, N', N-tetrameth-ylethylenediamine; AM = acrylamide; AA = acrylic acid; KPS = potassium peroxodisulfate.

Table 2. The preparation parameters and physicochemical properties of BCGs prepared by the co-pyrolysis.

Materials	Raw Materials and Pretreatment	Carbonization Process	SSA (m^2 g^{-1})	Morphology Features	Functional Group	Thermostability (TMLR)	pH_{PZC}	Ref.
Sisal leaves cellulose BCG	Cellulose in DI (1 wt%), then freeze-dried.	N_2 atmosphere, 5 °C/min, at 600 °C, 700 °C, 800 °C.	412, 457, 494	3D interconnection structure.	800 aerogel exclusively exhibits C-C bonds.	-	-	[49]
Chitosan BCG	Chitosan in KOH/urea/H_2O solvent, left to stand for 24 h and freeze-dried.	N_2 atmosphere, 5 °C/min, at 800 °C for 2 h.	2607	The 3D hierarchical porous structure.	-OH,C=O, and C-O-C were observed.	-	6.6	[13]
Chitosan BCG	Chitosan in KOH/urea/H_2O solution, repeat thawing–freezing and standing for 24 h, and finally freeze-drying.	N_2 atmosphere, 10 K/min (room temperature-773 K) and 5 K/min(773–1073K), stayed at 1073 K for 2 h.	1867	The honeycomb structure is formed by interconnecting the hierarchical pores.	Occurrence of -OH, amide II, and C-O-C characteristic peaks.	-	-	[9]
Hardwood pulp cellulose BCG	Mixed ChCl and glucose and added NMMO H_2O, VC, GA, and hardwood pulp, then stirred under vacuum at 90 °C, cooling and curing, and finally freeze-drying.	Ar atmosphere, 5 °C/min, at 400 °C for 2 h.	769	The surface appears wrinkled and the whole forms a 3D hierarchical porous network.	The aldehyde group of GA reacts chemically with the -OH group of cellulose to form the acetal group (O-C-O).	94.29%		[50]
Magnetic watermelon BCG	Watermelon placed in an autoclave and heated to produce gel monomers by hydrothermal reaction, freeze-drying, then embedded Fe_3O_4 in a network of gels.	N_2 atmosphere, at 550 °C for 4 h.	-	Catenulate carbon network and carbon nanosphere network; Fe_3O_4 nanoparticles were incorporated into the 3D porous networks of biochar aerogel.	Occurrence of characteristic peaks attributable to the Fe_3O_4 phase (JCPDS 75-0033).	C, O, and Fe elements were confirmed.	-	[51]
bacterial cellulose BCG	Dissolve D-glucose, yeast, peptone, and DHP in deionized water and adjusted pH = 5.0; inoculated with Acetobacter and then incubated statically at 30 °C, NaOH purified and washed, and finally freeze-dried.	N_2 atmosphere, 5 °C/min, at 1000 °C for 2 h.	375	Long filament nanofiber; 3D porous network structure.	-	-	-	[26]
Iron/cellulose BCG	Bamboo pulp in DI, $Fe(NO_3)_3 \cdot 9H_2O$ added, and finally freeze-dried.	N_2 atmosphere, 2 °C/min, at 240 °C for 1 h; then 2 °C/min, at 400 °C for 1 h; and 5 °C/min, at 800 °C for 2 h.	135	The surface is smooth, iron was distributed along the fibers, 3D porous network structure.	The -OH in the CA almost completely disappeared, but Fe-CA still showed a distinct -OH peak.	-	-	[52]

Table 2. *Cont.*

Materials	Raw Materials and Pretreatment	Carbonization Process	SSA (m^2 g^{-1})	Morphology Features	Functional Group	Thermostability (TMLR)	pH_{PZC}	Ref.
Carrageenan/sodium lignin sulfonate BCG	κ-Carrageenan (1 g) in DI, sodium lignin sulfonate added, then sealed crosslinking and freeze-drying.	N_2 atmosphere, 10 °C/min, at 550 °C for 0.5 h.	32.4	3D porous structure.	-	After carbonization, the C=C content is reduced.	-	[53]

ChCl = choline chloride; NMMO H_2O = N-methyl morpholine-N-oxide (NMMO) was further processed in a double glass reactor; VC = ascorbic acid; GA = glutaraldehyde; DHP = disodium hydrogen phosphate.

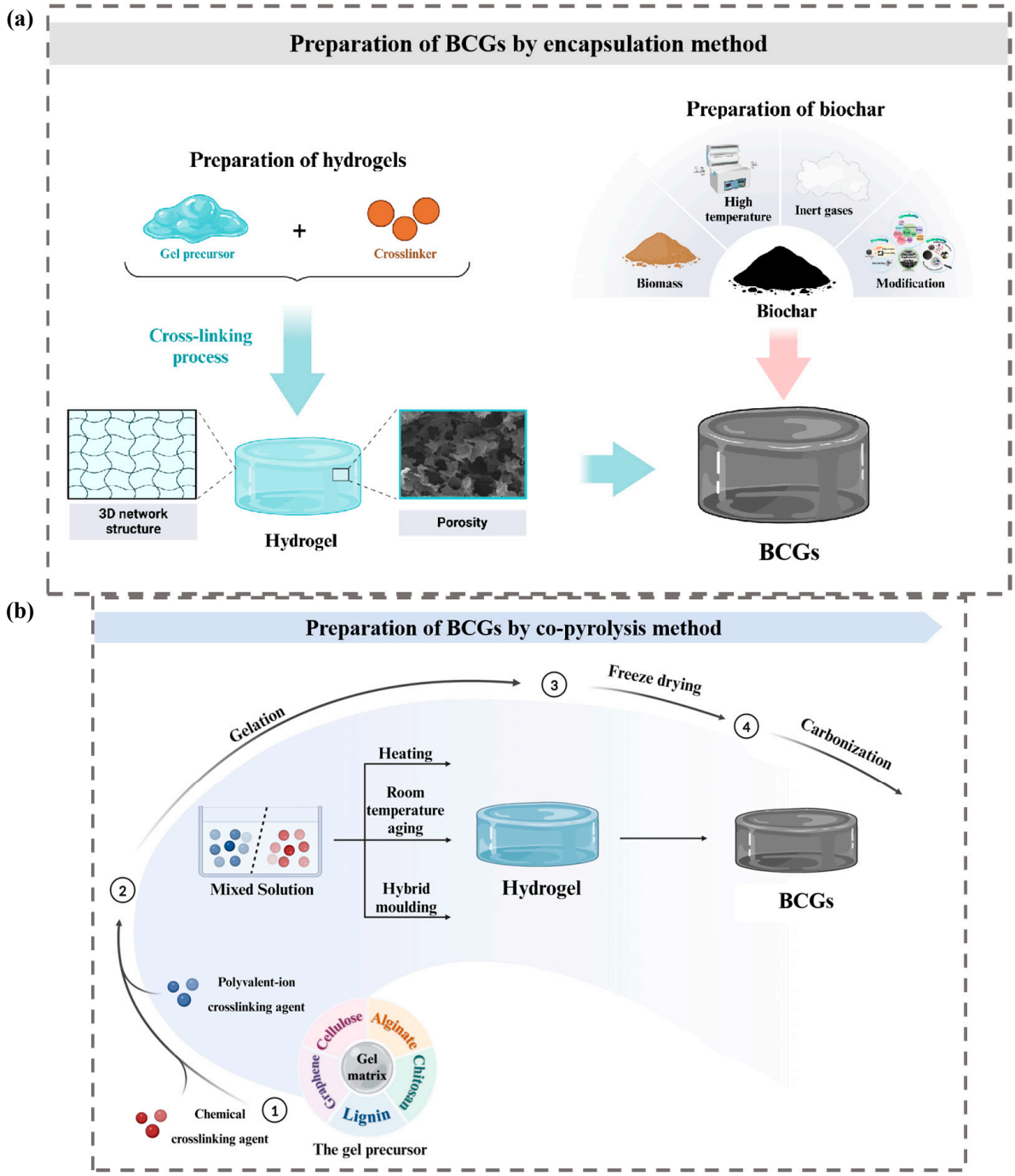

Figure 1. Process flow chart of BCGs prepared by (**a**) encapsulation and (**b**) co-pyrolysis. (**a**) Schematic illustrating the process of preparing BCGs using an encapsulation method. Initially, hydrogels are prepared by combining a gel precursor with a crosslinker, resulting in a cross-linking process that forms a three-dimensional network structure with porosity. Concurrently, biochar is produced from biomass through a process involving high temperature and inert gases, followed by modification. The biochar is then encapsulated within the hydrogel to form BCGs. This method ensures the integration of biochar properties within the hydrogel matrix, enhancing its functionality. (**b**) Schematic depicting the process of synthesizing BCGs using a co-pyrolysis method. Initially, a gel precursor is formed by combining cellulose, alginate, chitosan, or lignin with polyvalent-ion/chemical crosslinking agents. This mixture undergoes gelation to form a mixed solution (Step 1). Subsequently, the mixed solution is subjected to heating, which includes room temperature aging and hybrid molding, resulting in the formation of a hydrogel (Step 2). The hydrogel is then freeze-dried (Step 3) and further carbonized (Step 4) to produce BCGs.

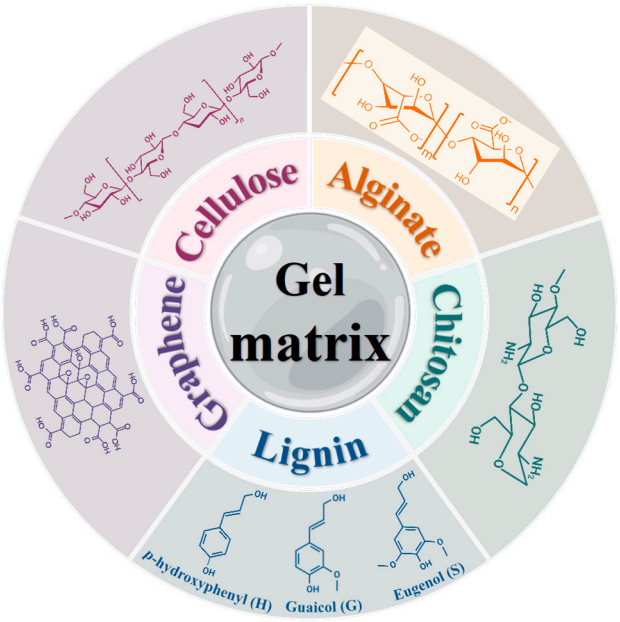

Figure 2. Main gel matrix types and their molecular structures of BCGs for water remediation applications. This diagram illustrates the main sources of the gel matrix, highlighting the chemical structure of these raw materials.

2.1. Cellulose-Based BCGs

2.1.1. Plant/Bacterial Cellulose-Based BCGs

Cellulose, a polymeric carbohydrate constituted by β-glycosidic linkages of D-glucose units, represents one of the most significant and bountiful biomass materials on Earth [54]. It is sourced from a variety of natural biomasses, including wood, leaves, bamboo, and cotton, or synthesized through microbial fermentation by organisms such as Acetobacter species [26,55,56]. Owing to its low cost, environmental compatibility, biodegradability, and high natural abundance, cellulose is regarded as a promising carbon-based material [57,58]. Compared to plant-derived cellulose, bacterial cellulose is a nanoscale cellulose with a larger specific surface area (SSA), higher purity, and superior crystallinity and tensile strength [59]. The purified bacterial cellulose hydrogel was subjected to freeze-drying followed by subsequent pyrolysis at 800 °C under an N_2 atmosphere [60]. The resulting bacterial cellulose BCG retains the interconnected fibrous network of the original microtubules, endowing it with a high porosity and voids. Moreover, its macroscopic size and lightweight architecture facilitate separation from solutions, rendering it advantageous for solid–liquid separation in practical applications.

However, it has been reported that BCGs synthesized from waste paper [61], cellulose nanofibers [26], bagasse [25], sponge gourd [62], and cotton [63] exhibit mechanical brittleness and incompressibility due to the poor thermal stability of their raw materials and their inherently random porous structures [26,57]. To date, numerous cellulose-based modified BCGs have been designed through alkali activation, 2,2,6,6-tetramethylpiperidine-1-oxyl (TEMPO) oxidation, and doping methods to enhance the structural stability and surface chemistry of pristine BCGs [61]. For instance, cellulose-based BCG derived from waste paper was further converted into activated BCG with excellent thermal stability and high specific surface area (654.58 m^2/g) via KOH alkali activation [61]. The alkali activation process not only preserves the cellulose structure but also provides larger diffusion channels and more adsorption functional groups for pollutants. Moreover, the activated cellulose-based BCG can be effectively regenerated through high-temperature combustion due to its enhanced thermal stability. The TEMPO oxidation method selectively oxidizes primary

alcohols in cellulose molecules into aldehydes and carboxyl groups, thereby reducing the degree of polymerization and increasing the content of oxygen-containing functional groups on the cellulose surface. Huang et al. (2020) obtained modified cellulose aerogels by subjecting bleached eucalyptus pulp to wet ball milling and TEMPO-mediated oxidation, followed by pyrolysis, resulting in modified cellulose BCG with an ultra-high specific surface area (2825 m^2 g^{-1}) and enhanced functional groups [33].

Metal particles, despite being highly efficient adsorbents, face significant limitations in large-scale applications due to challenges in separation and recovery, severe aggregation in aquatic environments, and potential risks to aquatic ecosystems and human health when leached into the environment [57]. On the one hand, cellulose gels, as precursors for porous BCGs, provide a three-dimensional network that serves as an excellent platform for stabilizing and immobilizing metal nanoparticles [26,64]. On the other hand, the doping of metal nanoparticles helps maintain the porous structure of cellulose-based BCGs during carbonization [26,64]. For instance, the in situ synthesis of monoclinic titanium dioxide (TiO_2(B)) within a cellulose-based BCG matrix has been reported to produce TiO_2(B)/cellulose aerogels, which were further pyrolyzed under N_2 conditions to obtain TiO_2(B)/cellulose BCG [64]. TiO_2(B) effectively enhances the stability of the cellulose BCG carbon skeleton, preserves the integrity of the porous structure during pyrolysis, and exposes more active adsorption sites. Similarly, ZIF-8-doped cellulose BCG was synthesized by leveraging the coordination between dimethylimidazole and Zn^{2+}, enabling the in situ synthesis of ZIF-8 nanoparticles on bacterial cellulose aerogels, followed by one-step carbonization [26]. The incorporation of ZIF-8 nanoparticles imparts a larger specific surface area, more N atoms, and hydrogen bonds between N atoms and water molecules, which are the primary reasons for the high adsorption capacity and hydrophilicity of TiO_2(B)/cellulose BCG. Ahamad et al. (2019) successfully developed N/S co-doped magnetic BCG using bagasse cellulose as the gel precursor and $FeCl_3$ and thiourea as modifiers through a combination of hydrothermal synthesis and subsequent carbonization [25]. This material exhibits a highly porous structure, enhanced chemical stability, and saturated magnetization properties. The presence of N/S groups improves the porosity, hydrophilicity, and selectivity of the N/S co-doped magnetic BCG, achieving a 99% removal rate for bisphenol-A. Moreover, the magnetic BCG can be easily separated under an external magnetic field, reducing the cost and time required for adsorbent separation. However, the extraction and processing costs of cellulose materials remain relatively high, and the dissolution process is complex and time-consuming due to the poor water solubility of cellulose, which continues to hinder its widespread application in aquatic environmental remediation [40,65].

2.1.2. Carboxymethyl Cellulose-Based BCGs

Carboxymethyl cellulose (CMC), a natural cellulose derivative, exhibits excellent properties, such as ease of regeneration, natural biodegradability, good biocompatibility, water solubility, and facile functionalization [42]. However, natural polymer gels often suffer from poor mechanical properties. By combining biochar as a carbon skeleton with CMC to prepare BCGs, the mechanical performance of the gel can be enhanced while addressing the challenge of separating biochar as an adsorbent. Yang et al. (2023) developed a green, stable, and highly efficient porous BCG by incorporating $KMnO_4$-modified cattail biochar with CMC and guar gum through free radical polymerization [42]. The doping of $KMnO_4$-modified cattail biochar improved the thermal stability and mechanical properties of the BCG and increased adsorption sites. However, studies have shown that the excessive addition of $KMnO_4$-modified cattail biochar can cover active sites, leading to a significant

decline in adsorption capacity. Therefore, modifying the composition of CMC-based BCG to achieve long-term stable adsorption of pollutants is both challenging and meaningful.

CMC contains abundant hydrophilic groups, and the chelation between carboxyl groups on its molecular chains and metal ions can promote gelation and enhance adsorption performance, which is not only simple and time-efficient but also non-toxic and environmentally friendly [40,65]. Using CMC, D-(+)-gluconic acid lactone, sodium montmorillonite, and $FeCl_3$ as raw materials, a 3D porous magnetic CMC/sodium montmorillonite BCG was synthesized through sol–gel, freeze-drying, and pyrolysis processes [65]. The magnetic CMC/sodium montmorillonite BCG exhibited stable oil adsorption capacity even after five adsorption-combustion cycles. Additionally, $FeCl_3$, as a crosslinking agent, endowed the CMC/sodium montmorillonite BCG with excellent magnetization properties, facilitating its adsorption and recovery. Yu et al. (2018) selected $FeCl_3$ as a crosslinking agent and collagen as an N source and mixed CMC with D-(+)-gluconic acid lactone, followed by freeze-drying and carbonization, to synthesize N-doped magnetic CMC BCG [41]. Further, KOH activation at 800 °C endowed the N-doped magnetic CMC BCG with a high specific surface area (589.6–664.3 $m^2\ g^{-1}$). The results indicated that the presence of Fe_3O_4, as well as pyridinic and pyrrolic nitrogen on the N-doped magnetic CMC BCG, facilitated adsorption, making the material more suitable for adsorbing cationic dyes such as malachite green and methylene blue. Using $Al_2(SO_4)_3$ as a crosslinking agent, CMC and D-(+)-gluconic acid lactone were mixed with plasticizer glycerol, and BCG was synthesized through freeze-drying and stepwise carbonization [40]. The irregular wrinkled surface of the BCG was likely caused by the crosslinking between CMC and Al^{3+}. Subsequently, the prepared BCG was converted into activated BCG through high-temperature KOH activation at 900 °C. Longer activation times resulted in higher specific surface areas and, consequently, greater dye adsorption capacities.

2.2. Alginate-Based BCGs

Sodium alginate (SA), a naturally occurring anionic polysaccharide, is rich in -COOH and -OH groups [28,38]. It rapidly forms hydrogels through a complexation mechanism when reacting with divalent cations (Ca^{2+}, Cu^{2+}, Zn^{2+}) and trivalent cations (Fe^{3+}) [32,66]. Due to its biocompatibility and cost-effectiveness, Ca^{2+} has become a widely used gelling agent for crosslinking with alginate, thereby enhancing the immobilization of carbon materials [29]. Therefore, powdered biochar adsorbents can be encapsulated within alginate-based gels to address the issues of biochar migration with water and insufficient adsorption sites [28,43]. During encapsulation, biochar, with good electrical conductivity, can be interpenetrated by long-chain alginate molecules to construct an interpenetrating polymer network, enhancing the electron transfer capability of the hydrogel and thereby increasing the surface reactivity of the BCGs [32]. SA was used to encapsulate ball-milled biochars derived from straw, distiller's grains, and Eupatorium adenophorum, respectively, and then dripped into $CaCl_2$ solution to form alginate-based BCG. The immobilization of ball-milled biochar within calcium alginate (CA) gel matrices enables its effective separation and recovery from water [29]. In a similar approach, CA was employed to embed biochars derived from Laminaria japonica, Undaria pinnatifida, and Porphyra tenera [29]. Both studies investigated the removal of phosphates, revealing that biochar synthesized from marine macroalgae and combined with SA-based BCG exhibited a higher binding affinity for phosphate pollutants due to stronger divalent cation bridging effects and higher Ca/P and Mg/P ratios. Hydroxyapatite-modified biochar prepared using hydroxyapatite and water hyacinth biomass can be further synthesized with SA to create hydroxyapatite-modified biochar/CA BCG, thereby enhancing the surface-active adsorption sites of the BCG [44]. Gao et al. (2023) impregnated cotton stalk biomass with $KMnO_4$ solution, followed by pyrolysis to synthesize $KMnO_4$-modified biochar, which was

mixed with SA colloid and dripped into $CaCl_2$ solution to induce the formation of spherical BCG through strong chelation [43]. The results showed that $KMnO_4$-modified biochar/CA BCG possessed a 3D hierarchical porous structure and richer oxygen-containing functional groups (-OH and -COOH). Using $FeCl_3$ and $FeSO_4$ as magnetic precursors, magnetic peanut shell biochar loaded with Fe_3O_4 was synthesized via the co-precipitation method, which was then used as a filler to fabricate superparamagnetic biochar/CA BCG [34]. Wu et al. (2023) used calcium sulfate-loaded bamboo biochar as a carrier, mixed it with polyethyleneimine (PEI) and SA in a specific ratio, and added glutaraldehyde solution to crosslink and synthesize biochar/PEI/CA composite BCGs under the action of Ca^{2+} ions [39]. PEI, with its abundant amine groups, exhibited excellent chelation capacity for heavy-metal ions [38]. Zhao et al. (2021) prepared BCG with excellent pH buffering capacity using pinewood biochar, sodium alginate, and $FeCl_3$ as a crosslinker via a sol–gel method [32]. Overall, the successful combination of biochar and alginate facilitates the regulation of surface functional groups, porous structure, and pH dependency in alginate-based BCGs.

2.3. Chitosan-Based BCGs

Chitosan (CS), derived from chitin through deacetylation, is a polysaccharide composed of β-(1-4)-linked glucosamine and N-acetylglucosamine residues, featuring an abundance of $-NH_2$ and -OH groups. CS can form gels with certain substances through chemical crosslinking and/or physical crosslinking, making it a promising candidate as a carrier for immobilizing biochar [11,67]. This approach could potentially enhance the chemical affinity and mechanical stability of biochar.

Interestingly, research has revealed that CS-based BCGs, which are applied in the field of water treatment, are typically constructed in alkaline solutions. These BCGs exhibit excellent high strength and biocompatibility [4,11]. Afzal et al. dissolved CS in an acetic acid solution and then added pomelo peel biochar to form a mixture, which was dropped into a NaOH solution to synthesize spherical BCG composites [11]. It was found that this BCG exhibited excellent chemical stability, and the effect of temperature on its adsorption performance was negligible. Biochar/CS BCGs were synthesized by dispersing biochar derived from the ficus macrocarpa branch in CS solutions of varying concentrations, followed by crosslinking with glutaraldehyde under alkaline conditions [4]. The results indicate that an increased proportion of glutaraldehyde enhances the crosslinking effect, thereby improving the stable binding between biochar and CS. Wang et al. (2023) employed a similar method to encapsulate nanoscale ZVI-modified biochar within a CS gel, resulting in a material that exhibits stable adsorption performance for Cr(VI) across a broad pH range [45]. The fabrication of alkali-activated biochar/CS BCG involves the incorporation of alkali-activated corncob biochar into CS, followed by cross-linking with epichlorohydrin to react with the hydroxyl groups of CS [67]. The embedding of alkali-activated biochar enhances the mechanical strength and porous structure of the BCG.

It has also been reported that CS gel can be directly employed as a precursor for the synthesis of BCG. Liu et al. (2019) dissolved CS in a KOH/urea/water system to form a gel precursor, which was subsequently freeze-dried and subjected to high-temperature carbonization, resulting in a BCG with a large SSA of 2607 $m^2\ g^{-1}$ [13]. Luo et al. initiated the process by using KOH and urea as CS gel agents, then added acetic acid to construct a gel form, and successfully prepared a CS-based BCG through a combination of hydrothermal carbonization and low-temperature oxidation treatment [68].

2.4. Lignin-Based BCGs

Lignin, the second most abundant natural polymer after cellulose, is derived from the secondary cell walls of plants [35]. Over 50 million tons of lignin are produced annually

from by-products of the paper industry, with more than 95% of this industrial lignin being underutilized [69]. Porous BCG materials prepared from lignin or lignin-derived monomers retain their original structural and surface chemical properties, exhibiting large SSA and high porosity, making lignin a promising low-cost precursor for BCGs [35,70].

The synthesis of $LaFeO_3$/lignin BCG was achieved by the crosslinking of $Fe(NO_3)_3$, $La(NO_3)_3$, citric acid, and lignin in a mixed solvent of deionized water and ethanol under heating conditions, followed by drying and carbonization at 600 °C [35]. The integration of adsorption by the lignin-based BCG with the Fenton-like photocatalytic process of $LaFeO_3$ significantly improves the degradation efficiency of ofloxacin, increasing it from 53.4% for pure $LaFeO_3$ to 95.6% for the $LaFeO_3$/lignin BCG composite. Sodium lignosulfonate and Kappa-Carrageenan (κ-Car) served as the raw materials for the synthesis of BCGs [53]. After being mixed and sealed for 24 h, the preparation was freeze-dried to convert into a BCG precursor. This precursor was then soaked in a KOH solution, followed by drying and co-pyrolysis to synthesize an alkali-activated κ-Car/lignin BCG with a substantial SSA of 594.6 $m^2\ g^{-1}$ and a 3D hierarchical porous structure. The study by Jiao et al. (2022) confirmed that the incorporation of sulfomethylated lignin (SL) significantly enhances the mechanical flexibility of MgO/CMC/SL BCG [57]. MgO nanoparticles, CMC, and SL are initially dispersed together in deionized water. The mixture is then subjected to directional freeze-drying to form a composite aerogel, which is subsequently pyrolyzed under N_2 to produce MgO/CMC/SL BCG with an ordered wavy-layered structure and excellent compressibility.

2.5. Graphene-Based BCGs

Graphene gels, in contrast to conventional polymer gels, are three-dimensional porous network structures composed of graphene nanosheets as the base element through lamellar stacking and cross-linking and have a large specific surface area, abundant multilevel pore structure, excellent biochemical inertness, and good mechanical strength [15,27]. Graphene oxide (GO) is an oxide of graphene that maintains the characteristic layered structure and large SSA of its graphene. By incorporating ethylenediamine as a nitrogen source into a mixture of magnetic shrimp shell biochar and GO, a gelation process was induced under heat [15]. Subsequent microwave drying yielded N-doped magnetic biochar/GO BCG. The results showed that the SSA of the N-doped magnetic biochar/GO BCG increased by 259.59 $m^2\ g^{-1}$ compared to the magnetic biochar alone, enhancing their affinity for Cr(VI) ions in aqueous solutions.

Research has demonstrated that the oxygen functional groups present in GO can be eliminated or diminished through chemical or thermal reduction processes, thereby restoring the sp^2 hybridized carbon network of graphene to form reduced graphene oxide (rGO) with enhanced thermal and mechanical stability [27]. In recent years, lightweight rGO aerogels have emerged as a focal point in graphene-based material research due to their large SSA, exceptional chemical stability, and three-dimensional porous architecture [27,71]. Che et al. enhanced the structural stability of a composite gel by incorporating polyvinyl alcohol into a ball-milled cotton stalk biochar/GO suspension [71]. Subsequently, the glutaraldehyde was employed as a cross-linking agent to facilitate the condensation reaction between the components. After a five-cycle freeze–thaw process, the composite gel precursor was immersed in an ascorbic acid solution, a reducing agent, and subsequently freeze-dried to yield ball-milled biochar/rGO BCG with a stable 3D structure and high porosity. The results confirmed that the specific surface area of BC-doped rGO aerogel was increased (13.74–17.65 $m^2\ g^{-1}$) compared to rGO aerogel, and its ability to adsorb Cr(VI) was increased threefold. Iron-loaded bagasse biochar was introduced into a GO suspension containing sodium citrate, a reducing agent, and self-assembled to form an iron-loaded biochar/rGO BCG under heat. Density functional

theory calculations confirmed that the rGO coating stabilized the anchoring of iron-activated species on the biochar, enhancing electron transfer efficiency and dispersion capacity, which in turn promoted its adsorption capacity [27]. BET analysis confirmed that biochar/rGO BCG and iron-modified biochar/rGO BCG exhibit higher specific surface areas and pore volumes compared to biochar alone. Although the GO/rGO matrix provides an excellent porous structure and large surface area favorable for adsorption in BCGs, its high cost and complex preparation process have limited its widespread application in treating water pollutants [71].

2.6. Other Types of BCG

In the realm of water treatment, the gel matrix in BCG composites, in addition to the main types mentioned above, exists, a number of which remain less explored. For example, the preparation of gellan gum-based BCG, via the solution-casting method, involved dispersing O. aegyptiaca biochar into a mixture containing gellan gum, polyvinyl alcohol, and glycerol, followed by drying the mixture in a petri dish [46]. Gellan gum can react with polyvinyl alcohol to form a gel, which constructs a polymer network. Glycerol serves as a cross-linking agent in the encapsulation of pea pod biochar within starch hydrogels, yielding adsorbents with superior stability [17]. Anionic esterified starch, in the presence of glutaraldehyde, can be a complex with cationic gelatin to encapsulate $CoFe_2O_4$ nanoparticles. Subsequently, $CoFe_2O_4$/starch-gelatin hybrid hydrogels and MoO_3-modified mallow stem biochar were mixed, milled, and subjected to microwave heating to prepare a BCG with supermagnetic properties [48].

In summary, BCGs enhance mechanical stability, porous structure, and surface chemistry by integrating the multiple advantages of biochar and gel matrices. However, the preparation process of BCGs is relatively complex, involving biochar production, hydrogel synthesis, and their integration, which increases production costs. To achieve large-scale applications, the development of more efficient and cost-effective production processes is essential.

3. Water Treatment

3.1. Removal of Organic Contaminants

Organic pollutants, such as dyes, phenols, pesticides, and antibiotics, pose significant environmental concerns due to their complex aromatic structures, high toxicity, and resistance to biodegradation [72,73]. In aquatic environments, these pollutants may undergo processes like hydrolysis and photolysis, potentially generating secondary toxicants or persisting as harmful residues. The adsorption of organic pollutants by BCGs can be attributed to several mechanisms: (1) π–π interaction: BCGs possess surfaces enriched with π-electrons from polycyclic aromatic structures (or with specific regions lacking π-electrons), which can interact with aromatic rings or lone pairs of electrons in organic molecules to form π/n-π-electron donor–acceptor (EDA) interactions; (2) hydrogen bonding: carboxyl and polar functional groups in organic molecules tend to form hydrogen bonds with oxygen-containing or other functional groups on the BCG's surface; (3) electrostatic interaction: electrostatic attraction arising from opposite charges between the adsorbent surface and organic adsorbates; (4) pore-filling: the 3D porous structure of BCGs facilitates the attachment of organic pollutants; and (5) hydrophobic interaction: organic pollutants with higher hydrophobicity in aqueous solutions can strongly adsorb onto hydrophobic BCGs' surfaces or pores [46,67,73,74] (Figure 3a). In this paper, some representative examples have been selected to highlight the viability and advantages of BCGs in the removal of organic pollutants. Table 3 provides a summary of BCG applications for the elimination of organic pollutants from aqueous solutions. Afzal et al. (2018) and Chen et al. (2021) respectively reported the adsorption performance of biochar/CS BCG and H_3PO_4-activated biochar/CA

BCG for ciprofloxacin, identifying the various mechanisms involved in the adsorption of ciprofloxacin onto BCGs, including π–π interactions, hydrogen bonding, hydrophobic interactions, electrostatic interactions, and pore filling, with maximum adsorption capacities of 80.29 and 97.10 mg g^{-1}. Both adsorbents maintained good adsorption capacities after multiple adsorption–desorption cycles, making them cost-effective options for removing ciprofloxacin from water. Therefore, to further enhance the removal efficiency of BCGs for various organic pollutants, it is crucial to consider multiple adsorption mechanisms, including π–π interactions, hydrogen bonding, electrostatic interactions, and pore filling. First of all, by tuning the aromaticity and graphitization degree of BCGs, their π–π interactions with aromatic organic pollutants can be enhanced. For example, BCGs pyrolyzed at high temperatures typically exhibit higher graphitization degrees, enabling more effective adsorption of aromatic pollutants such as polycyclic aromatic hydrocarbons [33]. Alkali activation can increase the graphitic crystallite domain size, further enhancing the π–π EDA interactions between BCGs and methylene blue [53].

(**a**)

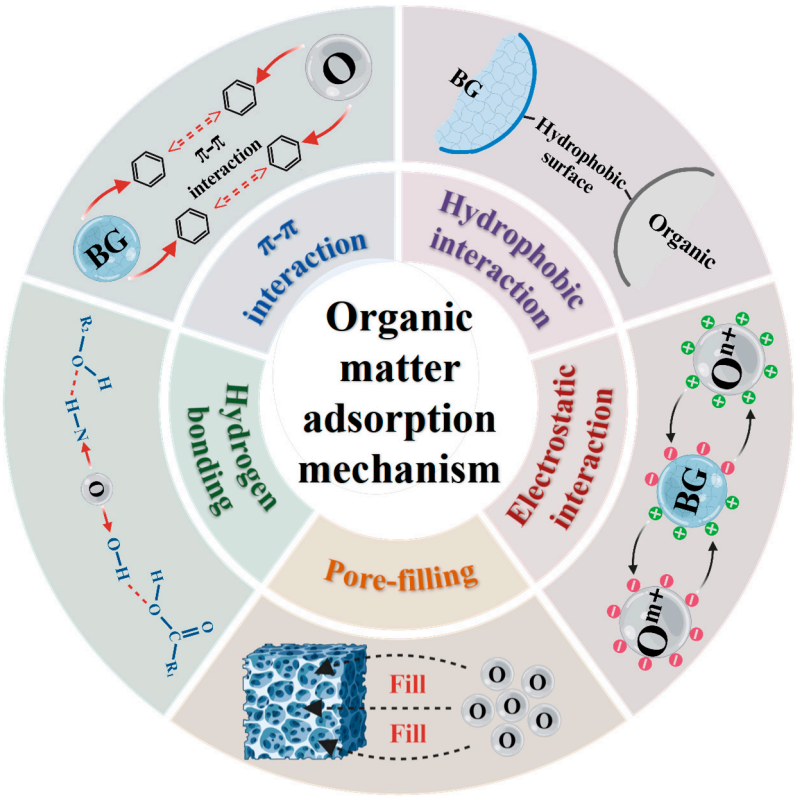

Figure 3. *Cont.*

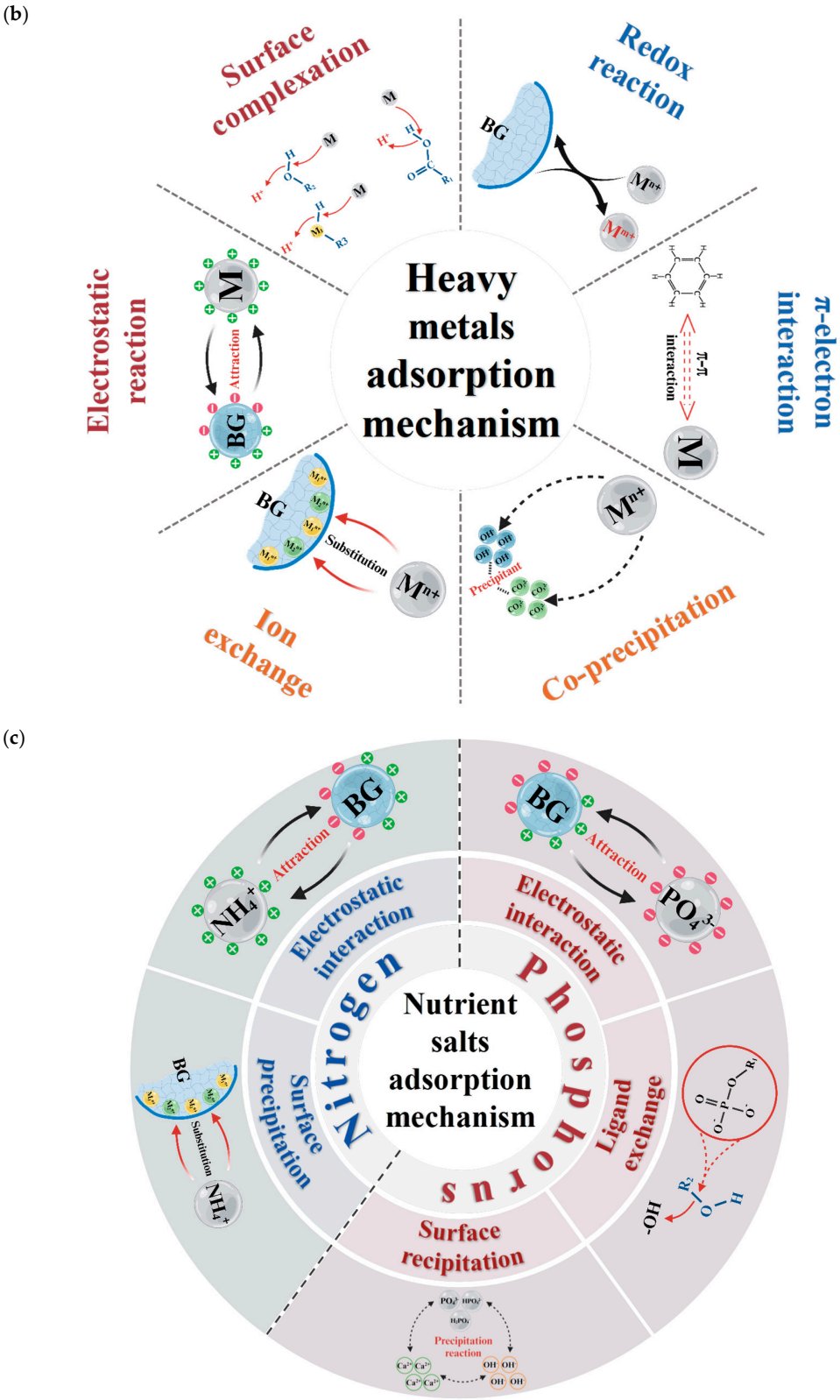

Figure 3. Adsorption mechanisms of (**a**) organics, (**b**) heavy metals, and (**c**) nutrient pollutants in water by BCG composites. (**a**) illustrates the various mechanisms, including hydrophobic interactions, π–π interactions, hydrogen bonding, electrostatic interactions, and pore-filling, by which organic matter is adsorbed onto BCGs. (**b**) depicts the mechanisms involved in the adsorption of heavy metals onto BCGs, which include ion exchange, complexation, electrostatic interactions, and co-precipitation. (**c**) illustrates the mechanisms, including electrostatic interactions, surface precipitation, and complexation, by which nutrient salts are adsorbed onto BCGs.

Table 3. The application and adsorption performance of BCGs for organic pollutants in aquatic remediation.

Materials	Pollutants	Dosage	Initial Concentration (mg L^{-1})	Adsorption Conditions	Q_m (mg g^{-1})	Isotherm	Reusability	Optimum pH	Main Mechanisms	Ref.
Bacterial cellulose	Methylene blue	0.5	50–110	25 °C	106.3	Langmuir	-	~12	Electrostatic interaction, π–π stacking, hydrogen bonds	[60]
	P-nitrophenol	0.5	50–110	25 °C	60.2	Freundlich	-	~2	π–π interaction, hydrogen bonding	
Sodium lignin sulfonate/κ-Carrageenan	Methylene blue	-	50–500	-	1330.68	Freundlich	-	11	Hydrogen bonding, π–π-electron donor–acceptor interaction, electrostatic interaction	[53]
Starch/biochar	Naproxen drug	1	5–50	50 min	309.82	Langmuir	5 cycles, no significant changes	2.0	Electrostatic attraction, pore filling, π–π interaction, and H-bonding	[17]
Chitosan	Chloramphenicol	0.25	20–200	25 °C 12 h	786.1	Langmuir-Freundlich	5 cycles, >87.5%	-	The pore-filling effect, π–π/ n-π EDA interaction and electrostatic interaction, hydrogen bonding interaction	[13]
	Florfenicol				751.5		5 cycles, >87.5%	-		
	Thiamphenicol				691.9		5, >80.0%	-		
Chitosan/biochar	Ciprofloxacin	5	5–160	20 °C	80.290	Langmuir	6 cycles, >64.0%	3.0	π–π-electron donor–acceptor (EDA) interaction, hydrogen bonding, and hydrophobic interaction	[11]
Sodium alginate//H_3PO_4 activated biochar	Ciprofloxacin	0.4	10–50	25 °C	97.10	Langmuir	5, 78%	6	Hydrogen bonding, π–π interaction, electrostatic interaction, hole filling	[74]
CMC/guar gum/$KMnO_4$-modified biochar	Methylene blue	0.2	25–175	-	598.28	Langmuir	5 cycles, >82.0%	6.0	Surface complexation and electrostatic attraction	[42]
Gellan gum/biochar	Methylene blue	-	0.0313 to 3.13 mmol MB L 1	25 °C 150 min	1.93 mmol g^{-1}	Sips	6, Loss at 6th/1st cycle: −4.8 %	10.5	Electrostatic interaction, π–π stacking, hydrogen bonds.	[46]
κ-carrageenan/calcium alginate/HKUST-1modified rice husk biochar	Tetracycline	0.9	10–200	24 h,	313.00	Freundlich	-	4.0	Hydrogen bonding, electrostatic attraction, metal–organic complexation, and π–π interaction	[75]
κ-carrageenan/calcium alginate/HKUST-1 modified wheat straw biochar			10–200		396.09	Freundlich	-	4.0		
Chitosan/biochar/Fe_3O_4	Tetracycline hydrochloride	-	-	-	206.98	Sips	-	6	Space-filling, hydrogen bonding, π–π interaction, electrostatic interaction and ion exchange	[76]
Chitosan/activated biochar	Anti-inflammatory drug ketoprofen	0.2	5–50	-	130.29	Langmuir	5, 51.47 mg g^{-1}	4	Hydrogen bonding, π–π interaction, electrostatic interaction, hole filling	[67]
Sugarcane bagasse-based cellulose	Bisphenol-A	5	10–250	25 °C	199.8	Langmuir	6, 21.9%	7	π–π interaction, hydrogen bonding	[25]
Polyacrylamide/wood biochar	Phenol	1	5–50	-	23.14	Langmuir	-	10	-	[22]
Polyacrylamide/chicken biochar				-	21.83,			-		
Polyacrylamide/tire biochar				-	14.04			-		
$CoFe_2O_4$ modified corn starch and gelatin/MoO_3 modified biochar	Doxorubicin	1.5	10–100	30 min	46.1187	Langmuir	5, 97.96	6	-	[77]
Polyvinyl alcohol/porous carbon	Congo red	-	40–80	-	160.47	Freundlich	3, the adsorption capacity could still maintain about 70% of the original	5	Hydrogen bond, electrostatic attraction	[78]
	Ibuprofen	-	10–50	-	45.75	Freundlich		~2.5		
	Doxycycline hydrochloride	-	10–30	-	36.59	Freundlich		4		

Introducing functional groups containing O/N (e.g., carboxyl, hydroxyl, amino) can enhance hydrogen bonding interactions between BCGs and organic pollutants, particularly for pollutants with polar functional groups. It has been reported that the -COOH and -OH groups on the surface of bacterial cellulose-based BCGs can promote interactions with methylene blue through hydrogen bonding, while hydrogen bonds can also form between its polar functional groups and p-nitrophenol [60]. The hydrogen bonding between the -OH groups of CS-based BCGs and the polar groups (i.e., -F, -Cl) of phenicol antibiotics provides a certain advantage in anion interference experiments [13]. The amino and thiol functional groups introduced in N/S-doped magnetic cellulose-based BCG facilitate hydrogen bonding interactions with the -OH groups of bisphenol-A, achieving a maximum adsorption capacity of 199.8 mg g^{-1} for bisphenol-A [25]. Additionally, surface modification can alter the surface charge of BCGs, thereby enhancing electrostatic interactions with charged organic pollutants. The TEMPO-mediated oxidation process introduces more oxygen-containing functional groups, reducing the surface charge of cellulose-based BCGs and favoring electrostatic attraction with cationic methylene blue and electrostatic repulsion with anionic alizarin reds. Furthermore, by tuning the pore structure of BCGs, their adsorption and diffusion capacities for organic pollutants of varying molecular sizes can be optimized. For example, alkali-activated sodium lignosulfonate/κ-carrageenan BCG and cellulose-based BCG subjected to continuous ball milling-oxidation exhibit hierarchical microporous–mesoporous–macroporous structures, which enhance methylene blue adsorption capacity through pore filling [33,53].

Finally, it was found that heavy-metal modification can further optimize the adsorption performance of BCGs for organic pollutants through surface complexation. Yu et al. (2022) reported the ability of HKUST-1/κ-carrageenan/calcium alginate/biochar BCG to remove tetracycline (TC), where the introduced Cu(I)/Cu^0 can form metal–organic complexes with the hydroxyl and amino groups of TC [75]. This, in combination with the inherent hydrogen bonding of BCG, π–π interactions, and electrostatic interactions, achieves a high adsorption capacity for TC (396.09 mg g^{-1}). Fe_3O_4 modification and CS gelation significantly enhanced the adsorption capacity of sludge-based biochar, with the prepared Fe_3O_4/CS/biochar BCG exhibiting a high adsorption capacity of 206.98 mg g^{-1} for tetracycline hydrochloride in aqueous solutions [76]. This is mainly attributed to (1) the dominant role of Fe_3O_4 surface complexation in adsorbing tetracycline hydrochloride, (2) hydrogen bonding interactions between the -NH_2 groups in CS and tetracycline hydrochloride, and (3) the transformation of BCG into a honeycomb-like porous structure due to the incorporation of Fe_3O_4 and CS, providing ample space for loading tetracycline hydrochloride. In summary, by synergistically optimizing the above-mentioned multiple adsorption mechanisms, BCGs can more efficiently remove various organic pollutants from water.

However, heavy-metal doping may pose a risk of secondary pollution, especially in acidic or oxidative environments, where heavy metals may leach from BCGs and cause potential environmental hazards [34]. Additionally, the introduction of heteroatoms may increase the complexity and cost of material preparation, limiting their widespread application in practice.

3.2. Removal of Heavy Metals

Heavy metal (HM) contamination is a pervasive environmental concern due to its high toxicity, persistence, non-biodegradability, and bioaccumulation potential [79]. The transport of HMs in aquatic environments is influenced by solubility, deposition, and complexation reactions, leading to unpredictable distribution and exposure patterns [72]. The extensive interconnected porosity and surface functional groups of BCG enhance the

adsorption of HM pollutants from water bodies [56,80]. Table 4 provides a summary of the removal performance and mechanisms of various biochar gel composites for heavy-metal pollutants. The adsorption of HM ions on BCG is primarily governed by surface complexation, electrostatic interactions, ion exchange, co-precipitation, π-electron interactions, and redox processes [71,81] (Figure 3b). Surface functional groups, such as hydroxyl, carboxyl, and amino groups, play a critical role in the adsorption of heavy metals by BCGs. For instance, the negatively charged hydroxyl and carboxyl groups commonly present in biochar/alginate BCG can attract positively charged metal ions through electrostatic interactions while also forming stable metal–organic complexes via coordination [34] (Equations (1)–(3)). The $KMnO_4$-modified biochar/calcium alginate BCG with an interconnected porous structure exhibits a maximum adsorption capacity of 664.6 mg g^{-1} for Pb(II) [43]. This is primarily attributed to electrostatic attraction between its negatively charged surface and positively charged Pb(II), as well as complexation, ion exchange, and precipitation involving hydroxyl, carboxyl groups, and exchangeable cations. Furthermore, Tao et al. (2024) confirmed that Pb(II) preferentially binds to -COOH groups over -OH groups in biochar/alginate biochar gels during adsorption [82]. The N atoms in amino functional groups can provide lone pair electrons, enabling coordination with metal cations [39,42]. Additionally, chemical modification to introduce specific functional groups can further enhance selective adsorption for certain heavy metals. Zhang et al. (2019) investigated the phosphate functionalization of graphene-based BCGs, where the abundant phosphate groups on the surface selectively bind to U(VI) through enhanced electrostatic interactions and surface complexation, increasing the adsorption capacity from 102.7 mg g^{-1} to 150.3 mg g^{-1} [83]. Moreover, Ji et al. (2023) incorporated hydroxyapatite-modified biochar into calcium alginate gels to increase metal hydroxide groups on the material surface [44]. The introduced metal hydroxides were found to play a significant role in the adsorption of Cd^{2+} and Pb^{2+} through complexation. The Fe-O group in iron-modified biochar/CA BCG forms stable coordination complexes with Cu(II), effectively enhancing the adsorbent capacity [84]. However, under strongly acidic conditions, the adsorption capacity of iron-modified biochar/CA BCG for Cu(II) is significantly reduced due to Fe leaching, limiting their application [34]. Numerous studies have shown that, in addition to surface complexation and electrostatic interactions, the adsorption mechanism of biochar/CA BCG for heavy-metal cations also includes ion exchange between metal cations and Ca^{2+} [34,84]. Furthermore, biochar doped within alginate gels can effectively promote the adsorption of heavy-metal cations (e.g., Pb(II)) through coordination bonds formed between the π-electron systems of aromatic rings and heavy-metal ions [44].

$$2R_1COO_{(S)}{}^{-} + M_{(aq)}{}^{2+} \leftrightarrow [(R_1COO^{-})_2M^{2+}]_{(S)} \quad (1)$$

$$2R_1O_{(S)} + M_{(aq)}{}^{2+} \leftrightarrow [(R_1O^{-})_2M^{2+}]_{(S)} \quad (2)$$

$$2R_2OH_{(S)} + M_{(aq)}{}^{2+} \leftrightarrow [(R_2O^{-})_2M^{2+}]_{(S)} + 2H^{+} \quad (3)$$

Table 4. The application and adsorption performance of BCGs for heavy-metal contaminants in aquatic remediation.

Materials	Pollutants	Dosage (mg L^{-1})	Initial Concentration (mg L^{-1})	Adsorption Conditions	Q_m (mg g^{-1})	Isotherm	Reusability	Optimum pH	Main Mechanisms	Ref.
Alginate/KOH-activated biochar	Pb(II)	0.5	100–500	25 °C, 12 h	294.90	Langmuir	7 cycles, still maintained 90.54% of the initial adsorption capacity of the original	6	Ion exchange, complexation,	[82]
$CoFe_2O_4$ modified corn starch and gelatin/MoO_3 modified biochar	Pb(II)	20	0.05–0.15	30 min	555.56	Langmuir	5 cycles, >85.0%	7.0	Complex formation ion exchange, catalytic reduction	[48]
Alginate/$KMnO_4$-modified biochar	Pb(II)	1	100–1000	35 °C, 24 h	664.60	Langmuir	-	-	Complexation, ion exchange, precipitation, and π-bonding.	[43]
Polyacrylamide/MnO_2 modified biochar	Pb(II)	0.3	2–50	25 °C, 24 h,	70.90	Freundlich	5 cycles, 80.5% of the initial adsorption capacities	-	Electrostatic attraction, ion exchange	[37]
	Cd(II)	0.3	2–50	25 °C, 24 h	84.76	Freundlich	5 cycles,92.1% of the initial adsorption capacities	-		
Alginate/hydroxyapatite-modified biochar	Pb(II) Cd(II)	0.3 0.3	10–200 10–200	25 °C, 24 h 25 °C 24 h	564.50 302.20	Langmuir Langmuir	-	-	Ion exchange, surface complexation, precipitation, and C-interaction	[44]
Polyethyleneimine/sodium alginate/calcium sulphate modified biochar	Cd(II)	-	50–500	25 °C, 24 h	151.98	Langmuir	Q_e value remained almost unchanged after four cycles	4	Surface complexation, ion exchange, and cation-π-bonding interactions.	[39]
Ferric alginate/biochar	Pb(II)	1	10–150	24 h	796.27	Langmuir	-	2.0.0	Surface complexation and precipitation.	[32]
	Cr(VI)				27.86	Freundlich	-	2.0–7.0	Electrostatic attraction, reduction, and surface complexation mechanisms	
Alginate/halloysite nanotubes/biochar	Pb(II) Cu(II) Ni(II) Cd(II)	3	0.5–80	25 °C, 12 h	26.49 6.96 16.87 2.85	Langmuir		8.5	Ion exchange, electrostatic interaction, pore filling	[80]
CMC/guar gum/$KMnO_4$-modified biochar	Cu(II) Co(II)	0.2	100–700 100–700	-	805.45 772.52	Langmuir	5 cycles, >82.0%	6.0	Surface complexation and electrostatic attraction	[42]
	Cu(II)	1	5–200	30 °C	234.1	Langmuir	3 cycles, 55.3%	6.0	Ion exchange, Van der Waals force, surface complexation	[34]
Cellulose	Cu (II)	0.4	400	12 h	801.00	-	-	-	-	[85]
Polyacrylamide/ZnO-modified biochar	U(VI)	0.5	0–30	-	239.21 (313 K)	Freundlich	5 cycles, 78.9%	5.0	Ion exchange and chelation	[47]
Chitosan/polyethyleneimine/biochar	U(VI)	0.1	5–150	1 h	633.40	Sips	3 cycles, 95.9%	4.0 −9.0	Electrostatic interaction, surface complexation, and ionization-precipitation	[86]
N-doped graphene oxide/Fe-modified biochar	Cr(VI)	2		25 °C, 30 min	348.36	Langmuir	8 cycles,88.6%,	1.0	Electrostatic adsorption (ion-pair), pore filling, reduction and coordination	[15]
Reduced graphene oxide/ball-milled biochar	Cr(VI)	1	10–100	25 °C, 12 h	39.97	Langmuir		2	Ion exchange, electrostatic interaction, reduction	[71]
nZVI@NCA900	Cr (VI)	1	20–600	25 °C, 24 h	176.53	Sips	7 cycles, it retained more than 87.5% of its original Cr (VI) adsorption performance.	2	Electrostatic interaction, reduction, and precipitation	[79]
Starch/biochar	Cr(VI)	1	5–50	30 min	420.13	Langmuir	5 cycles, no significant changes	1.0	Electrostatic attraction, redox reaction	[17]
Reduced graphene oxide/KOH-modified biochar	Cr(VI)	0.6	10–200	35 °C, 4 h	232.56	Langmuir		2.0	Electrostatic interaction, redox, and complexation	[10]
Polyethylene Imide/alginate/Nano-zero-valent iron-modified biochar	Sb(III)	0.2	50–300	25 °C, 5	509.34	L-F	5 cycles, it retained more than 90.6% of its original Sb (III) adsorption performance.	6	Oxidation, inner-sphere complexation, and co-precipitation	[38]
Alginate/La/Fe metal–organic frameworks biochar	Sb(III)	0.2	50–150	25 °C, 24 h	277.80	Freundlich		6	Hydrogen bonding and metal–organic complexation interactions	[81]
Chitosan/biochar	Sb(III)	2	-	25 °C, 24 h	168.00	Langmuir	3.70%	2	Electrostatic interaction, chelation, surface complexation, π–π interaction, and hydrogen bonding	[4]
Graphene oxide/Fe- modified biochar	Sb(III)	1	0–200	25 °C, 24 h	113.1	Freundlich	5 cycles, >85%	2	Surface complexation and π–π stacking	[27]

Redox reactions have been identified as a critical mechanism for the effective adsorption of variable-valent metal ions such as Cr(VI) and Sb(III) by BCGs. These reactions facilitate the transformation of these ions to less toxic or more easily adsorbable forms, thereby enhancing their removal efficiency. For instance, Che et al. (2022) demonstrated enhanced interactions between BC/rGA and Cr(VI), attributed to the participation of delocalized π-electrons from reduced graphene oxide in the reduction of Cr(VI) to Cr(III) (reduction reactions shown in Equations (4) and (5) [71]. Zhao et al. (2021) utilized Fe^{3+} as a crosslinker for biochar/ferric alginate biochar gels, endowing the material with a positively charged surface and excellent pH buffering capacity, while the conductivity of Fe^{3+} facilitated the reduction of Cr(VI) [32]. The resulting Cr(III) exhibited a high affinity for cationic functional groups on the material surface (e.g., protonated -COOH and -OH groups) and could be further immobilized on the BCG through ion exchange or surface complexation mechanisms (Equations (6) and (7)) [32,71]. Chen et al. (2022) investigated the adsorption of Sb(III) in water using biochar/CS BCG. The results showed that biochar/CS BCG, with its abundant active groups (e.g., C=O, -NH_2, and -OH), achieved a maximum adsorption capacity of 168 mg g^{-1} for Sb(III) through mechanisms including electrostatic interactions, chelation, surface complexation, π–π interactions, and hydrogen bonding, as well as enhanced redox capacity, significantly higher than the 10 mg g^{-1} of pristine biochar [4]. Chen et al., (2024) synthesized Fe/graphene nanosheet-loaded biochar, which promoted the oxidation of Sb(III) to Sb(V) (49.3–78.5%), likely due to the incorporation of Fe(III) or the contribution of surface radicals (Equation (8)) [27]. The graphene nanosheets enhanced electron transfer efficiency and dispersion, accelerating the oxidation of Sb(III). Introducing nano zero-valent iron (nZVI) during the preparation of biochar gels can mitigate aggregation issues and provide multiple redox sites [87]. Xue et al. (2021) uniformly loaded nZVI onto biochar gels, resulting in a synergistic effect of oxygen-containing groups, Fe^0 and Fe^{2+}, that promoted the reduction of Cr(VI) (Equations (9)–(11)) [52]. Wu et al. (2024) prepared nZVI-modified biochar/calcium alginate biochar gels using a sol–gel method. The nZVI facilitated the oxidation of Sb(III) to the less toxic Sb(V) (Equations (12)–(14)), followed by adsorption and co-precipitation of Sb(V) by iron oxide corrosion products [38].

$$HCrO_4^- + 7H^+ + 3e^- \rightarrow Cr^{3+} + 4H_2O \quad (4)$$

$$Cr_2O_7^{2-} + 14H^+ + 6e^- \rightarrow 2Cr^{3+} + 7H_2O \quad (5)$$

$$R\text{-}COOH + Cr^{3+} \rightarrow R\text{-}COO(Cr^{3+}) + H^+ \quad (6)$$

$$OH + Cr^{3+} \rightarrow R\text{-}O\text{-}Cr^{3+} + H^+ \quad (7)$$

$$2Fe^{3+} + Sb(OH)_3 + 3H_2O \rightarrow 2Fe^{2+} + Sb(OH)_6^- + 3H^+ \quad (8)$$

$$Fe + H^+ \rightarrow Fe^{2+} + R\ (R = e^-/H^*) \quad (9)$$

$$Cr(VI) + R \rightarrow Cr(III) \quad (10)$$

$$Cr(VI) + Fe^{2+} \rightarrow Cr(III) + Fe^{3+} \quad (11)$$

$$Fe(0) + O_2 + 2H^+ \rightarrow Fe(II) + H_2O_2 \quad (12)$$

$$Fe(II) + H_2O_2 \rightarrow \cdot OH + OH + Fe(III) \quad (13)$$

$$Sb(III) + \cdot OH \rightarrow Sb(V) + 2e^- \quad (14)$$

However, these optimization strategies face several challenges in practical applications. For example, at lower pH values, H^+ competes with metal cations for adsorption sites, while at higher pH values, OH^- forms precipitates with metal cations, both leading to reduced adsorption performance [43]. Additionally, in complex aquatic environments, the

coexistence of multiple metal ions can trigger competitive adsorption effects, significantly impacting the selective adsorption performance of BCGs. For instance, Pb(II) competes with target heavy-metal ions like Cd(II) for adsorption sites, reducing the adsorption capacity of calcium sulfate-modified biochar/polyethyleneimine/CA BCG for Cd(II) from 82.29 mg g^{-1} to 47.32 mg g^{-1} [39]. Therefore, future research must consider the design of surface functional groups, environmental conditions, and material cost-effectiveness to achieve the efficient and selective removal of HMs by BCGs in complex aquatic environments.

3.3. Removal of Nutrient Pollutants (P/N)

Nitrogen and phosphorus are crucial elements for the structure and function of living organisms [29]. However, their excessive inputs into aquatic environments can trigger eutrophication, leading to algal blooms and posing risks to drinking water safety and aquatic ecosystem biodiversity [28]. Table 5 provides a summary of the effects and mechanisms of phosphate and ammonium removal by various biochar gel composites, which typically possess an abundant mesoporous structure that enhances phosphorus adsorption. Current applications of biochar gel composites for phosphorus removal are primarily centered on alginate-based BCG. Ma et al. demonstrated that composites synthesized by coating biochar with a CS gel exhibit relatively weaker adsorption effects compared to calcium alginate gel [88]. This reduction in adsorption is attributed to a greater propensity for a decrease in SSA and the lack of surface precipitation of elemental calcium.

Alginate-based BCGs are extensively utilized for phosphorus removal, primarily due to two reasons: (1) Ligand exchange occurs between the -OH and -COOH groups on the BCG surface and the unprotonated oxygen atoms in PO_4^{3-}, which is a key process for phosphate adsorption by BCG [28,88]. Fourier-transform infrared (FTIR) spectroscopy confirms the disappearance of -OH functional groups on the surface of alginate-based BCG following phosphate adsorption, with a concurrent significant decrease in the intensity of functional groups such as C=O and C-O [25]. (2) Alginate uses metal ions as cross-linking agents during the biochar coating process, thereby incorporating metal elements onto the surface of the alginate-based BCG. This results in a surface with more positively charged and active sites on the BCG, which enhances the adsorption of phosphate anions through electrostatic interactions, surface precipitation, and ligand exchange [28,89]. The biochar/CA BCG synthesized using Ca^{2+} as a cross-linking agent was found to contain significantly enhanced Ca content on its surface by SEM-EDS scanning [28]. X-Ray diffraction (XRD) spectra indicated the formation of hydroxyapatite ($Ca_5(PO_4)_3OH$) after phosphate adsorption onto the biochar/CA BCG, confirming the presence of elemental Ca on the BCG surface and its role in the phosphate adsorption process through surface precipitation (Equations (15)–(17)). The use of Fe^{3+} and La^{3+} as cross-linking agents has been reported, where chemical coordination bonds (Fe-O-P and La-O-P) can form between Fe/La and P via Lewis acid-base interactions, leading to the substitution of -OH by P and the formation of an inner-sphere complex with strong ligand adsorption for P [89]. The adsorption efficiency of phosphorus can be further improved by enhancing the surface functionality of biochar/alginate BCG. BCG synthesized with magnesium-modified biochar encapsulated as a functional filler into CA matrices facilitated ligand exchange between Mg-OH and phosphate on their surfaces (Equation (18)) in addition to the formation of Ca-P precipitates ($Ca_3(PO_4)_2$) on their surfaces after adsorption (Equations (19)–(21)) [88]. Wang et al. discovered that polydopamine/CA/lanthanum-biochar composites engaged in ligand-exchange interactions of La-OH and electrostatic attraction involving protonated amino groups during phosphate adsorption [92]. Jiao et al. developed a MgO/SL/CMC composite with a maximum phosphate adsorption capacity of 218.51 mg g^{-1}, where MgO nanoparticles served as primary adsorption sites through ligand exchange with phosphate [57]. Overall,

the primary mechanisms for phosphate removal by biochar gel composites encompass electrostatic interactions, surface precipitation, and ligand exchange (Figure 3c).

$$5Ca^{2+} + 3PO_4^{3-} + OH^- \rightarrow Ca_5(PO_4)_3OH\downarrow \quad (15)$$

$$5Ca^{2+} + 3HPO_4^{2-} + 4OH^- \rightarrow Ca_5(PO_4)_3OH\downarrow + 3H_2O \quad (16)$$

$$5Ca^{2+} + 3H_2PO_4^- + 7OH^- \rightarrow Ca_5(PO_4)_3OH\downarrow + 6H_2O \quad (17)$$

$$2{\equiv}Mg\text{-}OH + H_2PO_4^- = ({\equiv}Mg)_2HPO_4 + H_2O + OH^- \quad (18)$$

$$3Ca^{2+} + 2PO_4^{3-} \rightarrow Ca_3(PO_4)_2\downarrow \quad (19)$$

$$3Ca^{2+} + 2HPO_4^{2-} + 2OH^- \rightarrow Ca_3(PO_4)_2\downarrow + 2H_2O \quad (20)$$

$$3Ca^{2+} + 2H_2PO_4^- + 4OH^- \rightarrow Ca_3(PO_4)_2\downarrow + 4H_2O \quad (21)$$

Overall, the primary mechanisms for phosphate removal by biochar gel composites encompass electrostatic interactions, surface precipitation, and ligand exchange (Figure 3c). The most influential factors in enhancing the phosphorus adsorption capacity of alginate-based BCGs include the type and modification of functional fillers (e.g., La-modified biochar, MgO nanoparticles), surface engineering (e.g., PDA coating), solution pH, and the presence of coexisting ions. Surface functional groups and metal ion cross-linking play crucial roles in the adsorption process for different phosphate species.

Limited research exists on the removal of nitrogen from water using BCGs. In one study, it was found that the ball-milled distiller grain biochar/CA BCG exhibited a maximum ammonium adsorption capacity of 12.27 mg g^{-1}, primarily through ion exchange (Equation (22)) and electrostatic attraction [28] (Figure 3c). Therefore, we can consider enhancing the electrostatic interactions between BCGs and ammonium ions by introducing more negatively charged functional groups (such as carboxyl and sulfonate groups) through surface modification. Additionally, doping with metal ions (e.g., Fe^{3+}, Al^{3+}) can improve the ion exchange capacity of biochar gels. For instance, Fe^{3+} can undergo ion exchange reactions with NH_4^+ to form stable complexes. Moreover, optimizing the pore structure and specific surface area of BCGs can also increase adsorption sites and enhance their adsorption kinetics.

$$BCG\text{-}M^{n+} + NH_4^+ \rightarrow BCG\text{-}NH_4^+ + M^{n+} \quad (22)$$

Overall, BCGs have demonstrated significant advantages in removing a variety of pollutants, yet their performance is highly dependent on material design and modification strategies. Future research should further optimize the surface chemistry, pore structure, and stability of these composites to enhance their application potential in real-world water remediation.

Table 5. The application and adsorption performance of BCGs for nutrient pollutants in aquatic remediation.

Materials	Pollutants	Dosage (mg g^{-1})	Initial Concentration (mg L^{-1})	Adsorption Conditions	Q_m (mg g^{-1})	Isotherm	Reusability	Optimum pH	Main Mechanisms	Ref.
Alginate/biochar	Phosphate	2	5–1000	30 °C, 24 h	157.70	Langmuir–Freundlich	-	6.0	Electrostatic attraction, Structural functional groups, and water molecules play an important role in phosphate adsorption	[29]
Alginate/Fe/La-modified biochar		2	25–100	25 °C, 24 h	46.65	Langmuir	5, 82%	6.0	Electrostatic attraction and ligand exchange	[89]
MgO-modified sulfonomethylated lignin/CMC			100–600	12 h	218.51	Langmuir	6, >81.95%	2–8	Ligand exchange	[57]
Mg-alginate/biochar		2	0–100	28 °C, 24 h	46.56	Langmuir	-	3–10	Surface precipitation and ligand exchange	[88]
Mg-chitosan/biochar		2	0–100	28 °C, 24 h	11.53	Freundlich	-	3–10	Surface precipitation and ligand exchange	
Alginate/Electrochemically-modified biochar		2.5	25–2000	30 °C, 24 h	342.67	Sips	-	4	Electrostatic attraction and ion exchange	[90]
Polyvinyl alcohol/alginate/La-modified biochar		0.5	10–100	25 °C, 24 h	13.74	Langmuir	5, 60%	4–6	Electrostatic attraction and ligand exchange	[89]
Alginate/Mg-modified biochar		10	0–2	25 °C, 160 min	20.32	Langmuir	5, 87.06%	-	Ligand exchange	[91]
Alginate/ball-milling rice straw biochar		0.5	20–300	25 °C, 24 h	31.80	Langmuir	-	10	Electrostatic attraction, surface precipitation, and ligand exchange	[28]
Alginate/ball-milling distillers grains biochar					24.10		-			
Alginate/ball-milling eupatorium adenophorum biochar					24.00		-			
Alginate/ball-milling rice straw biochar	Ammonium	0.5	27–407	25 °C, 24 h	10.15	S-shaped	-		Ion exchange and electrostatic attraction	
Alginate/ball-milling distillers grains biochar					12.27		-			
Alginate/ball-milling eupatorium adenophorum biochar					9.90		-			

4. Cost-Effectiveness Analysis of BCGs

4.1. Production Costs

The production cost of BCGs primarily includes raw material costs, energy consumption, equipment investment, and maintenance costs. The raw materials used in the production of BCGs, such as biomass and cross-linking agents, vary in price depending on their source and quality. For instance, the cost of biomass can be significantly reduced by using agricultural waste or other low-cost feedstocks. Energy consumption during the production process, particularly in the pyrolysis and drying steps, can be optimized by adopting energy-efficient technologies. Equipment investment and maintenance costs can be minimized by selecting appropriate production scales and equipment.

4.2. Application Costs

The application cost of BCGs in environmental remediation includes transportation, deployment, and monitoring costs. The transportation cost can be reduced by optimizing logistics and using local production facilities. Deployment costs can be minimized by developing efficient application methods and training personnel. Monitoring costs can be controlled by implementing cost-effective monitoring strategies and using advanced sensors.

5. Conclusions and Perspectives

This comprehensive review of BCG composites underscored their efficacy in environmental remediation, particularly in the context of water purification. The encapsulation and co-pyrolysis techniques offer distinct pathways to fabricating BCGs, and the prepared BCG showed superior integration and enhanced performance in the adsorptive removal of pollutants. Organic pollutants are primarily removed through π–π interactions, hydrogen bonding, electrostatic attraction, pore filling, and hydrophobic interactions with BCGs. In contrast, the mechanisms for heavy-metal removal by BCGs include surface complexation, electrostatic interactions, ion exchange, coprecipitation, π-electron interactions, and redox reactions. The removal of nutrient pollutants (P/N), particularly phosphate, by BCGs is mainly governed by electrostatic interactions, surface precipitation, and ligand exchange, while ammonium adsorption is predominantly controlled by ion exchange and electrostatic attraction.

Despite demonstrating excellent pollutant removal performance at the laboratory scale, the large-scale application of BCGs faces several challenges: (1) the complex synthesis processes and the need for precise control of reaction conditions can lead to increased production costs and difficulties in maintaining consistent product quality; (2) most gel precursors used in BCGs syntheses, such as cellulose, alginate, chitosan, and lignin, are biodegradable, which may lead to degradation in practical aquatic applications, compromising their long-term stability; (3) the potential environmental impact of cross-linking agents and the need for the efficient removal of residual chemicals are critical factors that must be addressed for large-scale production; (4) the performance of BCGs varies significantly under different environmental conditions, such as acidic or alkaline environments, where functional failure may occur; (5) the environmental safety of BCGs requires further evaluation, particularly regarding the potential release of by-products or degradation products and their impact on ecosystems.

To address these challenges, future research should focus on the following directions: Firstly, developing low-cost raw materials and green synthesis processes to reduce the production costs of BCGs; for example, utilizing agricultural waste or industrial by-products as biochar precursors or adopting low-temperature synthesis methods for hydrogels. Secondly, enhancing the mechanical strength and stability of BCGs by incorporating nanomaterials or crosslinking agents. Thirdly, the mechanisms underlying the performance variations of

BCGs under different environmental conditions need to be thoroughly investigated, and the development of more adaptable composite materials is also required. Furthermore, it is necessary to conduct analyses of the environmental footprint and lifecycle of BCGs. For example, the entire process of BCGs, from raw material acquisition to production processing, utilization, and disposal, should be thoroughly described. A comprehensive quantitative analysis using the LCA (Life Cycle Assessment) method should also be conducted, which is of significant importance for the sustainable production of BCGs. Lastly, the environmental impact differences between traditional materials and BCGs should be compared in terms of environmental, economic, and social factors to reinforce the sustainability assessment of BCGs.

Author Contributions: Conceptualization, H.W. and Z.F.; methodology, Y.Z.; investigation, Y.Z., C.W. and Q.H.; writing—original draft preparation, Y.Z., C.W. and Q.H.; writing—review and editing, Z.F., Y.G., H.C., J.C., J.L., X.Y., and H.W.; supervision, Z.F. and H.W. All authors have read and agreed to the published version of the manuscript.

Funding: This work was supported by the National Natural Science Foundation of China (42107031, 42207003), Natural Science Foundation of Guangdong Province, China (2024A1515011443), the Key Scientific and Technological Project of Foshan City (2120001008392), the Key project in Serving for Rural Revitalization of Department of Education of Guangdong Province, China (2019KZDZX2012), and the State Sponsored Postdoctoral Fellowship Programme (GZC20240324).

Data Availability Statement: No new data were created or analyzed in this study. Data sharing is not applicable to this article.

Acknowledgments: We would like to thank the reviewers and the editor-in-charge for their valuable time spent on this article. We also thank all the laboratory teams and foundations who have supported us.

Conflicts of Interest: The authors declare that they have no known competing financial interests or personal relationships that could have appeared to influence the work reported in this paper.

References

1. Asghar, N.; Hussain, A.; Nguyen, D.A.; Ali, S.; Hussain, I.; Junejo, A.; Ali, A. Advancement in nanomaterials for environmental pollutants remediation: A systematic review on bibliometrics analysis, material types, synthesis pathways, and related mechanisms. *J. Nanobiotechnol.* **2024**, *22*, 26. [CrossRef]
2. Fang, Z.; Gao, Y.; Wu, X.; Xu, X.; Sarmah, A.K.; Bolan, N.; Gao, B.; Shaheen, S.M.; Rinklebe, J.; Ok, Y.S.; et al. A critical review on remediation of bisphenol S (BPS) contaminated water: Efficacy and mechanisms. *Crit. Rev. Environ. Sci. Technol.* **2020**, *50*, 476–522. [CrossRef]
3. Heydari, M.; Amirjani, A.; Bagheri, M.; Sharifian, I.; Sabahi, Q. Eco-friendly pesticide based on peppermint oil nanoemulsion: Preparation, physicochemical properties, and its aphicidal activity against cotton aphid. *Environ. Sci. Pollut. Res.* **2020**, *27*, 6667–6679. [CrossRef] [PubMed]
4. Chen, H.; Gao, Y.; El-Naggar, A.; Niazi, N.K.; Sun, C.; Shaheen, S.M.; Hou, D.; Yang, X.; Tang, Z.; Liu, Z.; et al. Enhanced sorption of trivalent antimony by chitosan-loaded biochar in aqueous solutions: Characterization, performance, and mechanisms. *J. Hazard. Mater.* **2022**, *425*, 127971. [CrossRef] [PubMed]
5. Bolan, N.; Hoang, S.; Beiyuan, J.; Gupta, S.; Hou, D.; Karakoti, A.; Joseph, S.; Jung, S.; Kim, K.; Kirkham, M.; et al. Multifunctional applications of biochar beyond carbon storage. *Int. Mater. Rev.* **2021**, *66*, 1017–1054. [CrossRef]
6. Kunz Lazzari, L.; Perondi, D.; Zattera, A.J.; Campomanes Santana, R.M. Cellulose/Biochar Cryogels: A Study of Adsorption Kinetics and Isotherms. *Langmuir* **2021**, *37*, 3180–3188. [CrossRef]
7. Ohemeng-Boahen, G.; Sewu, D.D.; Woo, S.H. Preparation and characterization of alginate-kelp biochar composite hydrogel bead for dye removal. *Environ. Sci. Pollut. Res.* **2019**, *26*, 33030–33042. [CrossRef] [PubMed]
8. Shan, X.; Yang, L.; Zhao, Y.; Yang, H.; Xiao, Z.; An, Q.; Zhai, S. Biochar/Mg-Al spinel carboxymethyl cellulose-La hydrogels with cationic polymeric layers for selective phosphate capture. *J. Colloid Interface Sci.* **2022**, *606*, 736–747. [CrossRef]
9. Shang, W.; Liu, Y.; He, Q.; Liu, S.; Zhu, Y.; Tong, T.; Liu, B. Efficient adsorption of organic matters and ions by porous biochar aerogel as pre-treatment of ultrafiltration for shale gas wastewater reuse. *Chem. Eng. J. Adv.* **2020**, *2*, 100011. [CrossRef]

10. Wei, C.; Xiang, C.; Ren, E.; Cui, C.; Zhou, M.; Xiao, H.; Jiang, S.; Yao, G.; Shen, H.; Guo, R. Synthesis of 3D lotus biochar/reduced graphene oxide aerogel as a green adsorbent for Cr(VI). *Mater. Chem. Phys.* **2020**, *253*, 123271. [CrossRef]
11. Afzal, M.; Sun, X.; Liu, J.; Song, C.; Wang, S.; Javed, A. Enhancement of ciprofloxacin sorption on chitosan/biochar hydrogel beads. *Sci. Total Environ.* **2018**, *639*, 560–569. [CrossRef] [PubMed]
12. Hui, B.; Chen, H.; Zhou, C.; Cai, L.; Zhang, K.; Quan, F.; Yang, D. Biochar aerogel-based electrocatalyst towards efficient oxygen evolution in acidic media. *Biochar* **2022**, *4*, 39. [CrossRef]
13. Liu, H.; Wei, Y.; Luo, J.; Li, T.; Wang, D.; Luo, S.; Crittenden, J.C. 3D hierarchical porous-structured biochar aerogel for rapid and efficient phenicol antibiotics removal from water. *Chem. Eng. J.* **2019**, *368*, 639–648. [CrossRef]
14. Liu, Y.; Li, Y.; Huang, J.; Zhang, Y.; Ruan, Z.; Hu, T.; Wang, J.; Li, W.; Hu, H.; Jiang, G. An advanced sol-gel strategy for enhancing interfacial reactivity of iron oxide nanoparticles on rosin biochar substrate to remove Cr(VI). *Sci. Total Environ.* **2019**, *690*, 438–446. [CrossRef]
15. Mahmoud, M.E.; Mohamed, A.K.; Salam, M.A. Self-decoration of N-doped graphene oxide 3-D hydrogel onto magnetic shrimp shell biochar for enhanced removal of hexavalent chromium. *J. Hazard. Mater.* **2021**, *408*, 124951. [CrossRef] [PubMed]
16. Zhao, H.; Li, X.; Zhang, L.; Hu, Z.; Zhong, L.; Xue, J. Preparation and bacteriostatic research of porous polyvinyl alcohol / biochar / nanosilver polymer gel for drinking water treatment. *Sci. Rep.* **2021**, *11*, 12205. [CrossRef] [PubMed]
17. Mohamed, A.K.; Mahmoud, M.E. Nanoscale Pisum sativum pods biochar encapsulated starch hydrogel: A novel nanosorbent for efficient chromium (VI) ions and naproxen drug removal. *Bioresour. Technol.* **2020**, *308*, 123263. [CrossRef] [PubMed]
18. Zhou, Z.; Liu, Y.; Liu, S.; Liu, H.; Zeng, G.; Tan, X.; Yang, C.; Ding, Y.; Yan, Z.; Cai, X. Sorption performance and mechanisms of arsenic(V) removal by magnetic gelatin-modified biochar. *Chem. Eng. J.* **2017**, *314*, 223–231. [CrossRef]
19. Fang, Z.; Gao, Y.; Zhang, F.; Zhu, K.; Shen, Z.; Liang, H.; Xie, Y.; Yu, C.; Bao, Y.; Feng, B.; et al. The adsorption mechanisms of oriental plane tree biochar toward bisphenol S: A combined thermodynamic evidence, spectroscopic analysis and theoretical calculations. *Environ. Pollut.* **2022**, *310*, 119819. [CrossRef]
20. Fang, Z.; Gao, Y.; Bolan, N.; Shaheen, S.M.; Xu, S.; Wu, X.; Xu, X.; Hu, H.; Lin, J.; Zhang, F.; et al. Conversion of biological solid waste to graphene-containing biochar for water remediation: A critical review. *Chem. Eng. J.* **2020**, *390*, 124611. [CrossRef]
21. Wang, C.; Zhao, Y.; Gao, Y.; Chen, H.; Li, X.; Zhou, B.; Fan, D.; Fang, Z.; Liu, J. Interpretable machine learning for predicting heavy metal removal and optimizing biochar characteristics. *J. Water Process. Eng.* **2024**, *68*, 106484. [CrossRef]
22. Karakoyun, N.; Kubilay, S.; Aktas, N.; Turhan, O.; Kasimoglu, M.; Yilmaz, S.; Sahiner, N. Hydrogel–Biochar Composites for Effective Organic Contaminant Removal from Aqueous Media. *Desalination* **2011**, *280*, 319–325. [CrossRef]
23. Gao, Y.; Fang, Z.; Lin, W.; Chen, H.; Bhatnagar, A.; Li, J.; Xie, Y.; Bao, Y.; Chen, J.; Zhao, H.; et al. Large-flake graphene-modified biochar for the removal of bisphenol S from water: Rapid oxygen escape mechanism for synthesis and improved adsorption performance. *Environ. Pollut.* **2023**, *317*, 120847. [CrossRef] [PubMed]
24. Cheng, Y.; Li, A.; Shi, W.; Zhao, L. Magnetic chitosan-functionalized waste carton biochar composites for efficient adsorption of anionic and cationic dyes. *Chem. Eng. J.* **2024**, *481*, 148535. [CrossRef]
25. Ahamad, T.; Naushad, M.; Ruksana; Alhabarah, A.N.; Alshehri, S.M. N/S doped highly porous magnetic carbon aerogel derived from sugarcane bagasse cellulose for the removal of bisphenol-A. *Int. J. Biol. Macromol.* **2019**, *132*, 1031–1038. [CrossRef]
26. Ma, X.; Xu, Y. Three-dimensional porous nitrogen-doped carbon aerogels derived from cellulose@mof for efficient removal of dye in water. *J. Environ. Chem. Eng.* **2022**, *10*, 108385. [CrossRef]
27. Chen, H.; Gao, Y.; Fang, Z.; Li, J.; Pillai, S.C.; Song, H.; Sun, C.; Bolan, N.; Yang, X.; Vithanage, M.; et al. Investigating the electron-scale adsorption mechanisms using DFT calculations and experimental studies in self-assembly magnetic biochar gel incorporated with graphene nanosheets for enhanced Sb(III) removal. *Chem. Eng. J.* **2024**, *487*, 150740. [CrossRef]
28. Feng, Q.; Chen, M.; Wu, P.; Zhang, X.; Wang, S.; Yu, Z.; Wang, B. Simultaneous reclaiming phosphate and ammonium from aqueous solutions by calcium alginate-biochar composite: Sorption performance and governing mechanisms. *Chem. Eng. J.* **2022**, *429*, 132166. [CrossRef]
29. Jung, K.-W.; Jeong, T.-U.; Kang, H.-J.; Ahn, K.-H. Characteristics of biochar derived from marine macroalgae and fabrication of granular biochar by entrapment in calcium-alginate beads for phosphate removal from aqueous solution. *Bioresour. Technol.* **2016**, *211*, 108–116. [CrossRef] [PubMed]
30. Wan, Z.; Cho, D.-W.; Tsang, D.C.W.; Li, M.; Sun, T.; Verpoort, F. Concurrent adsorption and micro-electrolysis of Cr(VI) by nanoscale zerovalent iron/biochar/Ca-alginate composite. *Environ. Pollut.* **2019**, *247*, 410–420. [CrossRef] [PubMed]
31. Chen, H.; Gao, Y.; Li, J.; Fang, Z.; Bolan, N.; Bhatnagar, A.; Gao, B.; Hou, D.; Wang, S.; Song, H.; et al. Engineered biochar for environmental decontamination in aquatic and soil systems: A review. *Carbon Res.* **2022**, *1*, 4. [CrossRef]
32. Zhao, C.; Hu, L.; Zhang, C.; Wang, S.; Wang, X.; Huo, Z. Preparation of biochar-interpenetrated iron-alginate hydrogel as a pH-independent sorbent for removal of Cr(VI) and Pb(II). *Environ. Pollut.* **2021**, *287*, 117303. [CrossRef] [PubMed]
33. Huang, P.; Zhang, P.; Min, L.; Tang, J.; Sun, H. Synthesis of cellulose carbon aerogel via combined technology of wet ball-milling and TEMPO-mediated oxidation and its supersorption performance to ionic dyes. *Bioresour. Technol.* **2020**, *315*, 123815. [CrossRef]

34. Salem, D.B.; Ouakouak, A.; Touahra, F.; Hamdi, N.; Eltaweil, A.S.; Syed, A.; Boopathy, R.; Tran, H.N. Easy separable, floatable, and recyclable magnetic-biochar/alginate bead as super-adsorbent for adsorbing copper ions in water media. *Bioresour. Technol.* **2023**, *383*, 129225. [CrossRef]
35. Chen, X.; Zhang, M.; Qin, H.; Zhou, J.; Shen, Q.; Wang, K.; Chen, W.; Liu, M.; Li, N. Synergy effect between adsorption and heterogeneous photo-Fenton-like catalysis on LaFeO3/lignin-biochar composites for high efficiency degradation of ofloxacin under visible light. *Sep. Purif. Technol.* **2022**, *280*, 119751. [CrossRef]
36. Shen, Y.; Fang, Q.; Chen, B. Environmental applications of three-dimensional graphene-based macrostructures: Adsorption, transformation, and detection. *Environ. Sci. Technol.* **2015**, *49*, 67–84. [CrossRef]
37. Wu, Z.; Chen, X.; Yuan, B.; Fu, M.-L. A facile foaming-polymerization strategy to prepare 3D MnO2 modified biochar-based porous hydrogels for efficient removal of Cd(II) and Pb(II). *Chemosphere* **2020**, *239*, 124745. [CrossRef]
38. Wu, A.; Jia, X.; Zhang, K.; Shao, J.; Mao, J.; Yang, Z.; Duan, Z.; Chen, W.-T.; Chang, F.; Wang, S.; et al. Environmentally friendly zero-valent iron-modified biochar beads for high-performance antimonite removal from aqueous solution. *J. Clean. Prod.* **2024**, *460*, 142534. [CrossRef]
39. Wu, A.; Sun, R.; Zhang, D.; Zhou, S.; Liu, Q.; Ge, J.; Chen, J.; Hu, G. Separable calcium sulphate modified biochar gel beads for efficient cadmium removal from wastewater. *Int. J. Biol. Macromol.* **2023**, *252*, 126253. [CrossRef] [PubMed]
40. Yu, M.; Li, J.; Wang, L. KOH-activated carbon aerogels derived from sodium carboxymethyl cellulose for high-performance supercapacitors and dye adsorption. *Chem. Eng. J.* **2017**, *310*, 300–306. [CrossRef]
41. Yu, M.; Han, Y.; Li, J.; Wang, L. Magnetic N-doped carbon aerogel from sodium carboxymethyl cellulose/collagen composite aerogel for dye adsorption and electrochemical supercapacitor. *Int. J. Biol. Macromol.* **2018**, *116*, 1084–1092. [CrossRef] [PubMed]
42. Yang, L.; Bao, L.; Dong, T.; Xie, H.; Wang, X.; Wang, H.; Wu, J.; Hao, C. Adsorption properties of cellulose/guar gum/biochar composite hydrogel for Cu2+, Co2+ and methylene blue. *Int. J. Biol. Macromol.* **2023**, *242*, 125021. [CrossRef] [PubMed]
43. Gao, L.; Li, Z.; Yi, W.; Wang, L.; Song, N.; Zhang, W.; Li, G.; Wang, S.; Li, N.; Zhang, A. Effective Pb2+ adsorption by calcium alginate/modified cotton stalk biochar aerogel spheres: With application in actual wastewater. *J. Environ. Chem. Eng.* **2023**, *11*, 109074. [CrossRef]
44. Ji, Y.; Zheng, N.; Wu, B.; An, Q.; Li, Z.; Sun, S.; Zhang, W.; Li, X.; Wang, S. Novel modified wood ear mushroom sticks biochar aerogel spheres for efficient capture of Cd^{2+} and Pb^{2+} mix-ions from water. *Environ. Technol. Innov.* **2023**, *31*, 103206. [CrossRef]
45. Wang, T.; Sun, Y.; Bai, L.; Han, C.; Sun, X. Ultrafast removal of Cr(VI) by chitosan-coated biochar-supported nano zero-valent iron aerogel from aqueous solution: Application performance and reaction mechanism. *Sep. Purif. Technol.* **2023**, *306*, 122631. [CrossRef]
46. Elgarahy, A.M.; Mostafa, H.Y.; Zaki, E.G.; ElSaeed, S.M.; Elwakeel, K.Z.; Akhdhar, A.; Guibal, E. Methylene blue removal from aqueous solutions using a biochar/gellan gum hydrogel composite: Effect of agitation mode on sorption kinetics. *Int. J. Biol. Macromol.* **2023**, *232*, 123355. [CrossRef] [PubMed]
47. Guo, Y.; Liu, X.; Xie, S.; Liu, H.; Wang, C.; Wang, L. 3D ZnO modified biochar-based hydrogels for removing U(VI) in aqueous solution. *Colloids Surf. A Physicochem. Eng. Aspects* **2022**, *642*, 128606. [CrossRef]
48. Mahmoud, M.E.; Abouelanwar, M.E.; Mahmoud, S.E.M.E.; Salam, M.A. Doping starch-gelatin mixed hydrogels with magnetic spinel ferrite@biochar@molybdenum oxide as a highly efficient nanocomposite for removal of lead (II) ions. *J. Environ. Chem. Eng.* **2021**, *9*, 106682. [CrossRef]
49. Lv, Y.; Bao, J.; Dang, Y.; Liu, D.; Li, T.; Li, S.; Yu, Y.; Zhu, L. Biochar aerogel enhanced remediation performances for heavy oil-contaminated soil through biostimulation strategy. *J. Hazard. Mater.* **2023**, *443*, 130209. [CrossRef] [PubMed]
50. Ma, X.; Zhou, S.; Li, J.; Xie, F.; Yang, H.; Wang, C.; Fahlman, B.D.; Li, W. Natural microfibrils/regenerated cellulose-based carbon aerogel for highly efficient oil/water separation. *J. Hazard. Mater.* **2023**, *454*, 131397. [CrossRef] [PubMed]
51. Wu, X.-L.; Wen, T.; Guo, H.-L.; Yang, S.; Wang, X.; Xu, A.-W. Biomass-Derived Sponge-like Carbonaceous Hydrogels and Aerogels for Supercapacitors. *ACS Nano* **2013**, *7*, 3589–3597. [CrossRef] [PubMed]
52. Xue, X.; Yuan, W.; Zheng, Z.; Zhang, J.; Ao, C.; Zhao, J.; Wang, Q.; Zhang, W.; Lu, C. Iron-loaded carbon aerogels derived from bamboo cellulose fibers as efficient adsorbents for Cr(VI) removal. *Polymers* **2021**, *13*, 4338. [CrossRef]
53. Lv, D.; Li, Y.; Wang, L. Carbon aerogels derived from sodium lignin sulfonate embedded in carrageenan skeleton for methylene-blue removal. *Int. J. Biol. Macromol.* **2020**, *148*, 979–987. [CrossRef]
54. Senthil, C.; Lee, C.W. Biomass-derived biochar materials as sustainable energy sources for electrochemical energy storage devices. *Renew. Sustainable Energy Rev.* **2021**, *137*, 110464. [CrossRef]
55. Qasim, U.; Osman, A.I.; Al-Muhtaseb, A.H.; Farrell, C.; Al-Abri, M.; Ali, M.; Vo, D.-V.N.; Jamil, F.; Rooney, D.W. Renewable cellulosic nanocomposites for food packaging to avoid fossil fuel plastic pollution: A review. *Environ. Chem. Lett.* **2021**, *19*, 613–641. [CrossRef]
56. Zhang, L.; Guo, L.; Wei, G. Recent Advances in the Fabrication and Environmental Science Applications of Cellulose Nanofibril-Based Functional Materials. *Materials* **2021**, *14*, 5390. [CrossRef]

57. Jiao, G.-J.; Ma, J.; Zhang, J.; Zhou, J.; Sun, R. High-efficiency capture and removal of phosphate from wastewater by 3D hierarchical functional biomass-derived carbon aerogel. *Sci. Total Environ.* **2022**, *827*, 154343. [CrossRef] [PubMed]
58. Song, P.; Cui, J.; Di, J.; Liu, D.; Xu, M.; Tang, B.; Zeng, Q.; Xiong, J.; Wang, C.; He, Q.; et al. Carbon microtube aerogel derived from kapok fiber: An efficient and recyclable sorbent for oils and organic solvents. *ACS Nano* **2020**, *14*, 595–602. [CrossRef] [PubMed]
59. Li, D.; Tian, X.; Wang, Z.; Guan, Z.; Li, X.; Qiao, H.; Ke, H.; Luo, L.; Wei, Q. Multifunctional adsorbent based on metal-organic framework modified bacterial cellulose/chitosan composite aerogel for high efficient removal of heavy metal ion and organic pollutant. *Chem. Eng. J.* **2020**, *383*, 123127. [CrossRef]
60. Hosseini Talari, M.; Tabrizi, N.S.; Babaeipour, V.; Halek, F. Adsorptive removal of organic pollutants from water by carbon fiber aerogel derived from bacterial cellulose. *J. Sol-Gel Sci. Technol.* **2022**, *101*, 345–355. [CrossRef]
61. Ma, L.; Li, D.; Chen, X.; Xu, H.; Tian, Y. A sustainable carbon aerogel from waste paper with exceptional performance for antibiotics removal from water. *J. Hazard. Mater.* **2024**, *474*, 134738. [CrossRef]
62. Yang, H.; Sun, J.; Zhang, Y.; Xue, Q.; Xia, S. Preparation of hydrophobic carbon aerogel using cellulose extracted from luffa sponge for adsorption of diesel oil. *Ceram. Int.* **2021**, *47*, 33827–33834. [CrossRef]
63. Ma, X.; Dong, B.; Xie, F.; Yang, H.; Wang, C.; Bittencourt, C.; Snyders, R.; Li, W. A novel cost-effective kapok fibers and regenerated cellulose-based carbon aerogel for continuous oil/water separation. *Sep. Purif. Technol.* **2025**, *353*, 128435. [CrossRef]
64. Zhu, J.; Chen, S.; Ma, G.; Ren, J.; Li, H.; Lin, W.; Huang, H.; Li, Z. Regenerated cellulose as template for in-situ synthesis of monoclinic titanium dioxide nanocomposite carbon aerogel towards multiple application in water treatment. *J. Colloid Interface Sci.* **2023**, *630*, 772–782. [CrossRef]
65. Yu, M.; Han, Y.; Li, J.; Wang, L. Magnetic carbon aerogel pyrolysis from sodium carboxymethyl cellulose/sodium montmorillonite composite aerogel for removal of organic contamination. *J. Porous Mater.* **2018**, *25*, 657–664. [CrossRef]
66. Li, S.; Zhang, L.; Tian, S.; He, Y.; Guo, X. Mineralized cupric phosphate/alginate gel alternately multilayer-wrapped nanofibrous membrane with robust anti-crude oil pollution for oily wastewater purification. *J. Membr. Sci.* **2023**, *669*, 121280. [CrossRef]
67. Chen, J.; Ouyang, J.; Lai, W.; Xing, X.; Zhou, L.; Liu, Z.; Chen, W.; Cai, D. Synthesis of ultralight chitosan/activated biochar composite aerogel globules for ketoprofen removal from aqueous solution. *Sep. Purif. Technol.* **2021**, *279*, 119700. [CrossRef]
68. Luo, L.; Cheng, S.; Yue, L.; You, Z.; Cai, J. N-doped biochar from chitosan gel-like solution: Effect of hydrothermal temperature and superior aqueous Cr (VI) removal performance. *Colloids Surf. A Physicochem. Eng. Aspects* **2022**, *641*, 128426. [CrossRef]
69. Liu, Y.; Jin, C.; Yang, Z.; Wu, G.; Liu, G.; Kong, Z. Recent advances in lignin-based porous materials for pollutants removal from wastewater. *Int. J. Biol. Macromol.* **2021**, *187*, 880–891. [CrossRef]
70. Gao, X.; Ren, P.; Wang, J.; Ren, F.; Dai, Z.; Jin, Y. Fabrication of visible-light responsive TiO_2@C photocatalyst with an ultra-thin carbon layer to efficiently degrade organic pollutants. *Appl. Surf. Sci.* **2020**, *532*, 147482. [CrossRef]
71. Che, N.; Liu, N.; Li, Y.; Li, C.; Liu, Y.; Li, C.; 2022. Three dimensional BC/rGA aerogel: Preparation, characterization, and adsorption of Cr(VI). *Biochar* **2022**, *4*, 65. [CrossRef]
72. Liang, L.; Xi, F.; Tan, W.; Meng, X.; Hu, B.; Wang, X. Review of organic and inorganic pollutants removal by biochar and biochar-based composites. *Biochar* **2021**, *3*, 255–281. [CrossRef]
73. Qiu, B.; Shao, Q.; Shi, J.; Yang, C.; Chu, H. Application of biochar for the adsorption of organic pollutants from wastewater: Modification strategies, mechanisms and challenges. *Sep. Purif. Technol.* **2022**, *300*, 121925. [CrossRef]
74. Chen, J.; Ouyang, J.; Cai, X.; Xing, X.; Zhou, L.; Liu, Z.; Cai, D. Removal of ciprofloxacin from water by millimeter-sized sodium alginate/H3PO4 activated corncob-based biochar composite beads. *Sep. Purif. Technol.* **2021**, *276*, 119371. [CrossRef]
75. Yu, F.; Pan, J.; Li, Y.; Yang, Y.; Zhang, Z.; Nie, J.; Ma, J. Batch and continuous fixed-bed column adsorption of tetracycline by biochar/MOFs derivative covered with κ-carrageenan/calcium alginate hydrogels. *J. Environ. Chem. Eng.* **2022**, *10*, 107996. [CrossRef]
76. Zhou, B.; Sang, Q.; Wang, Y.; Huang, H.; Wang, F.; Yang, R.; Zhao, Y.; Xiao, Z.; Zhang, C.; Li, H. Comprehensive understanding of tetracycline hydrochloride adsorption mechanism onto biochar-based gel pellets based on the combination of characterization-based and approximate site energy distribution methods. *J. Clean. Prod.* **2023**, *416*, 137909. [CrossRef]
77. Mahmoud, M.E.; Ibrahim, G.A.A. Cr(VI) and doxorubicin adsorptive capture by a novel bionanocomposite of Ti-MOF@TiO_2 incorporated with watermelon biochar and chitosan hydrogel. *Int. J. Biol. Macromol.* **2023**, *253*, 126489. [CrossRef] [PubMed]
78. Zhang, M.; Yu, X.; Zhu, M.; Xiang, A.; Bai, Y.; Zhou, H. Adsorptive behaviors and mechanisms for removing three organic pollutants from aqueous solutions by polyvinyl alcohol/porous carbon composite hydrogels. *J. Environ. Chem. Eng.* **2023**, *11*, 111095. [CrossRef]
79. Li, J.; Xia, C.; Cheng, R.; Lan, J.; Chen, F.; Li, X.; Li, S.; Chen, J.; Zeng, T.; Hou, H. Passivation of multiple heavy metals in lead–zinc tailings facilitated by straw biochar-loaded N-doped carbon aerogel nanoparticles: Mechanisms and microbial community evolution. *Sci. Total Environ.* **2022**, *803*, 149866. [CrossRef]
80. Hassan, M.; Liu, Y.; Naidu, R.; Du, J.; Qi, F.; Donne, S.W.; Islam, M.M. Mesoporous Biopolymer Architecture Enhanced the Adsorption and Selectivity of Aqueous Heavy-Metal Ions. *ACS Omega* **2021**, *6*, 15316–15331. [CrossRef] [PubMed]

81. He, Y.; Sun, R.; Zhang, D.; Wang, Y.; Zhou, S.; Deng, X.; Wang, B.; Hu, G. Separable alginate gel spheres encapsulated with La-Fe modified biochar for efficient adsorption of Sb(III) with high capacity. *J. Hazard. Mater.* **2023**, *460*, 132322. [CrossRef]
82. Tao, S.; Lu, L.; Zhou, T.; Zhang, Y.; Guo, Y. Design of recoverable biochar/alginate gel and its removal performance for Pb(II) in water: Simulation and experiment. *J. Mol. Liq.* **2024**, *405*, 125042. [CrossRef]
83. Zhang, Z.; Dong, Z.; Wang, X.; Dai, Y.; Cao, X.; Wang, Y.; Hua, R.; Feng, H.; Chen, J.; Liu, Y.; et al. Synthesis of ultralight phosphorylated carbon aerogel for efficient removal of U(VI): Batch and fixed-bed column studies. *Chem. Eng. J.* **2019**, *370*, 1376–1387. [CrossRef]
84. Yu, C.; Wang, M.; Dong, X.; Shi, Z.; Zhang, X.; Lin, Q. Removal of Cu(II) from aqueous solution using Fe_3O_4–alginate modified biochar microspheres. *RSC Adv.* **2017**, *7*, 53135–53144. [CrossRef]
85. Wang, H.; Gong, Y.; Wang, Y. Cellulose-based hydrophobic carbon aerogels as versatile and superior adsorbents for sewage treatment. *RSC Adv.* **2014**, *4*, 45753–45759. [CrossRef]
86. Zhang, Y.; Mei, B.; Shen, B.; Jia, L.; Liao, J.; Zhu, W. Preparation of biochar@chitosan-polyethyleneimine for the efficient removal of uranium from water environment. *Carbohydr. Polym.* **2023**, *312*, 120834. [CrossRef]
87. Wang, L.; Wang, Y.; Ma, F.; Tankpa, V.; Bai, S.; Guo, X.; Wang, X. Mechanisms and reutilization of modified biochar used for removal of heavy metals from wastewater: A review. *Sci. Total Environ.* **2019**, *668*, 1298–1309. [CrossRef]
88. Cui, X.; Dai, X.; Khan, K.; Li, T.; Yang, X.; He, Z. Removal of phosphate from aqueous solution using magnesium-alginate/chitosan modified biochar microspheres derived from Thalia dealbata. *Bioresour. Technol.* **2016**, *218*, 1123–1132. [CrossRef] [PubMed]
89. He, D.; Zhang, Z.; Zhang, W.; Zhang, H.; Liu, J. Municipal sludge biochar skeletal sodium alginate beads for phosphate removal. *Int. J. Biol. Macromol.* **2024**, *261*, 129732. [CrossRef]
90. Jung, K.-W.; Jeong, T.-U.; Choi, J.-W.; Ahn, K.-H.; Lee, S.-H. Adsorption of phosphate from aqueous solution using electrochemically modified biochar calcium-alginate beads: Batch and fixed-bed column performance. *Bioresour. Technol.* **2017**, *244*, 23–32. [CrossRef] [PubMed]
91. Fu, X.; Wang, P.; Wu, J.; Zheng, P.; Wang, T.; Li, X.; Ren, M. Hydrocotyle vulgaris derived novel biochar beads for phosphorus removal: Static and dynamic adsorption assessment. *J. Environ. Chem. Eng.* **2022**, *10*, 108177. [CrossRef]
92. Wang, B.; Hu, X.; Li, L.; Xie, Y.; Chen, R.; Guo, W.; Wang, H.; Wang, M.; Shi, J.; Chen, L.; et al. Enhanced phosphate removal by filler encapsulation and surface engineering using SA/PVA matrix: Fabrication optimization, adsorption behaviors, and inner removal mechanism. *Chem. Eng. J.* **2023**, *472*, 145073. [CrossRef]